Monthly Notices
of the
ROYAL ASTRONOMICAL SOCIETY

Mon. Not. R. Astron. Soc. **412,** 561–579 (2011) doi:10.1111/j.1365-2966.2010.17928.x

A statistical comparison of the optical/UV and X-ray afterglows of gamma-ray bursts using the *Swift* Ultraviolet Optical and X-ray Telescopes

S. R. Oates,[1⋆] M. J. Page,[1] P. Schady,[1] M. De Pasquale,[1] P. A. Evans,[2] K. L. Page,[2] M. M. Chester,[3] P. A. Curran,[1] T. S. Koch,[3] N. P. M. Kuin,[1] P. W. A. Roming,[3] M. H. Siegel,[3] S. Zane[1] and J. A. Nousek[3]

[1]*Mullard Space Science Laboratory, University College London, Holmbury St. Mary, Dorking Surrey RH5 6NT*
[2]*X-ray and Observational Astronomy Group, Department of Physics and Astronomy, University of Leicester, Leicester LE1 7RH*
[3]*Department of Astronomy and Astrophysics, Pennsylvania State University, 104 Davey Laboratory, University Park, PA 16802, USA*

Accepted 2010 October 27. Received 2010 September 29; in original form 2010 February 17

ABSTRACT

We present the systematic analysis of the Ultraviolet/Optical Telescope (UVOT) and X-ray Telescope (XRT) light curves for a sample of 26 *Swift* gamma-ray bursts (GRBs). By comparing the optical/UV and X-ray light curves, we found that they are remarkably different during the first 500 s after the Burst Alert Telescope trigger, while they become more similar during the middle phase of the afterglow, i.e. between 2000 and 20 000 s.

If we take literally the average properties of the sample, we find that the mean temporal indices observed in the optical/UV and X-rays after 500 s are consistent with a forward-shock scenario, under the assumptions that electrons are in the slow cooling regime, the external medium is of constant density and the synchrotron cooling frequency is situated between the optical/UV and X-ray observing bands. While this scenario describes well the averaged observed properties, some individual GRB afterglows require different or additional assumptions, such as the presence of late energy injection.

We show that a chromatic break (a break in the X-ray light curve that is not seen in the optical) is present in the afterglows of three GRBs and demonstrate evidence for chromatic breaks in a further four GRBs. The average properties of these breaks cannot be explained in terms of the passage of the synchrotron cooling frequency through the observed bands, nor a simple change in the external density. It is difficult to reconcile chromatic breaks in terms of a single component outflow and instead, more complex jet structure or additional emission components are required.

Key words: gamma-ray burst: general.

1 INTRODUCTION

Gamma-ray bursts (GRBs) are intense flashes of gamma-rays that can last from as little as a few milliseconds up to a few thousand seconds after the trigger. The duration and spectral hardness distributions are found to be bimodal, leading to a division of GRBs into two classes: short-hard GRBs (<2 s) and long-soft GRBs (>2 s) (Kouveliotou et al. 1993). The prompt gamma-ray emission is expected to be followed by an afterglow. The afterglow is most commonly seen in the X-rays, but is also observed in the optical/UV and, less commonly, down to radio wavelengths. The duration of the afterglow in the X-ray and optical/UV band varies considerably from GRB to GRB, and it has been observed to last for as little as a few hours up to a few months after the trigger. In the radio, the afterglow emission may be detected up to several years after the prompt gamma-ray emission. The afterglow from a short GRB tends to be fainter and short-lived in comparison with the long GRBs. For this reason, only long GRBs fall into the Oates et al. (2009) selection criteria. This paper is the successor to Oates et al. (2009) and therefore uses the same sample of 26 GRBs.

Due to the unpredictability and rapid fading of these cosmic explosions, crucial clues on to their nature, their possible progenitors and their environments could only be obtained through deep and continuous observations of the afterglow. A rapid response satellite, *Swift*, which was launched in 2004 November, was specifically

⋆E-mail: sro@mssl.ucl.ac.uk

designed to observe these events. *Swift* houses three instruments designed to capture the gamma-ray, X-ray and optical/UV emission. The Burst Alert Telescope (BAT; Barthelmy et al. 2005) detects the prompt gamma-ray emission. The X-ray Telescope (XRT; Burrows et al. 2005) and the Ultraviolet/Optical Telescope (UVOT; Roming et al. 2005) observe the afterglow. The energy ranges of the BAT and the XRT instruments are 15–350 and 0.2–10 keV, respectively, and the wavelength range of the UVOT is 1600–8000 Å. The co-alignment of the XRT and UVOT instruments is ideal for observing GRB afterglows because observations of the X-ray and optical/UV afterglow are performed simultaneously.

One of the early results that emerged from the first 27 X-ray afterglows collected by *Swift* is the existence of a 'canonical' X-ray light curve, which typically comprises four segments (Nousek et al. 2006). Here and throughout the paper, we will use the flux convention $F \propto t^{\alpha}\,\nu^{\beta}$ with α and β being the temporal and spectral indices, respectively. With this notation, the canonical X-ray light curve can be described as an initial steep decay segment ($-5 < \alpha_{\rm X} < -3$) transitioning to a shallow decay phase ($-1.0 < \alpha_{\rm X} < 0.0$; Liang, Zhang & Zhang 2007), then followed by a slightly steeper decay ($-1.5 < \alpha_{\rm X} < -1.0$), which finally breaks again at later times. The last segment is usually identified as a post-jet-break decay (Zhang et al. 2006). However, the application of this model to all GRBs has recently been questioned by Evans et al. (2009) with a larger sample of 327 GRBs, 162 of which are considered by Evans et al. (2009) to be well sampled. This paper found that the 'canonical' behaviour accounts for only ∼42 per cent of XRT afterglows.

A statistical study of the UVOT light curves has recently shown that, although there are some similarities between the optical/UV and X-ray bands, in general the optical/UV afterglow does not behave in the same way as the X-ray one (Oates et al. 2009). In particular, the optical/UV light curves can either decay from the beginning of the observations or exhibit an initial rise and then a decay phase. In both cases, the decay segment is usually well fitted by a power law, although a small number of GRBs require a broken or a doubly broken power law. Moreover, by systematically comparing the optical/UV light curves with the XRT canonical model, Oates et al. (2009) found that among the four segments of the XRT canonical model the shallow decay segment has the most similar range of temporal indices to the optical/UV light curves. The temporal indices of the other segments of the XRT canonical light curve are steeper than the temporal indices of the optical/UV light curves.

In this paper, we present a statistical cross comparison of the XRT and UVOT light curves for a sample of 26 GRBs presented in Oates et al. (2009). Table 1 lists these GRBs and their respective redshifts. The paper is organized as follows. In Section 2 we describe the data reduction and analysis. The main results are presented in Section 3. Discussion and conclusions follow in Sections 4 and 5, respectively. All uncertainties throughout this paper are quoted at 1σ.

2 DATA REDUCTION AND ANALYSIS

The 0.3–10 keV X-ray light curves were obtained from the GRB light curve repository at the UK *Swift* Science Data Center (Evans et al. 2007, 2009). In order to directly compare the behaviour of the UVOT and XRT light curves, we required the bins in the XRT light curve to be small, allowing us to rebin the light curve so that the X-ray bins have the same start and end times as the corresponding bins in the UVOT light curve. In order to be able to use Gaussian statistics for error propagation (when performing background subtraction and corrections due to pile-up and removal of bad columns), the minimum binning provided by the XRT repository is 15 counts bin^{-1}. We set the binning to be a minimum of 15 counts bin^{-1} for both the windowed timing and photon counting modes and switched the dynamic binning option off. For some of the repository light curves the last data point has a detection of $<3\sigma$. These points are provided by the repository as an upper limit and are excluded from further analysis.

The optical/UV light curves were taken from Oates et al. (2009, see section 3.1 of that paper for a detailed description of the construction of the UVOT light curves). These light curves are normalized to the v filter and grouped with a bin size of $\Delta t/t = 0.2$. The X-ray data were then binned so that the X-ray bins had the same time ranges as the UVOT light-curve bins. The binned X-ray and v-band count rate light curves for each GRB can be seen in the top pane of each panel in Fig. 1.

In Oates et al. (2009), the start time of each UVOT light curve was taken to be the start time of the gamma-ray emission rather than the BAT trigger time. The start time of the gamma-ray emission we take to be the start time of the T_{90} parameter. This parameter corresponds to the time in which 90 per cent of the counts in the 15–350 keV band arrive at the detector (Sakamoto et al. 2008) and is determined from the gamma-ray event data for each GRB, by the BAT processing script. The results of the processing are publicly available and are provided for each trigger at http://gcn.gsfc.nasa.gov/swift_gnd_ana.html. Therefore, to have consistent start times, the XRT light curves were adjusted to have the same start times as the UVOT light curves.

We then applied three different techniques to the optical/UV and X-ray light curves to determine how their behaviour compares over the course of *Swift* observations; these techniques are described in Sections 2.1 to 2.3. To avoid having hardness ratios with errors larger than ± 1 and to avoid taking the logarithm of negative numbers when determining the rms deviation, we only use the binned data points with a signal-to-noise ratio >1 for these two methods. When determining the temporal indices we used all the available data.

2.1 Optical/UV to X-ray hardness ratio

To determine how the count rates in the optical/UV and X-ray light curves vary with respect to each other, we calculated the hardness ratio of the optical/UV and X-ray count rates. We define hardness ratio to be

$$\mathrm{HR} = (C_{\rm X} - C_{\rm O})/(C_{\rm X} + C_{\rm O}), \quad (1)$$

where $C_{\rm O}$ is the v-band count rate and $C_{\rm X}$ is the X-ray count rate. A hardness ratio equal to -1 indicates that the optical/UV flux is dominant, whereas a HR $= 1$ indicates that the X-ray flux is dominant. The X-ray and optical/UV light curves have comparable count rates which allow hardness ratios to be computed without significant portions of the hardness ratios being saturated. However, the hardness ratios can only provide information on the relative spectral change, which may be due to the passage of a synchrotron spectral frequency, differences in the emission mechanisms or differences in the emission geometry. The hardness ratios for each GRB can be seen in the middle pane of each panel in Fig. 1.

2.2 Rms deviation

To determine how closely the data points in the optical/UV and X-ray light curves track each other during a given epoch, we determined the rms of the difference between the logarithmic normalized

Table 1. Spectroscopic redshifts were largely taken from the literature. For four GRBs, photometric redshifts, indicated by an *, were determined using the XRT–UVOT SEDs (see Oates et al. 2009, for details). The table also displays the temporal indices for the optical/UV and X-ray light curves for the four epochs: <500, 500–2000, 2000–20 000and >20 000 s.

		Temporal Index							
		Optical/UV				X-ray			
GRB	Redshift	<500 s	500–2000 s	2000–20 000 s	>20 000 s	<500 s	500–2000 s	2000–20 000 s	>20 000 s
050319	3.24[a]	0.86 ± 1.33	−0.59 ± 0.34	−0.48 ± 0.20	−0.92 ± 0.16	−7.76 ± 1.17	−0.70 ± 0.23	−0.68 ± 0.14	−1.24 ± 0.11
050525	0.606[b]	−1.28 ± 0.04	−0.97 ± 0.10	−0.91 ± 0.07	−1.18 ± 0.09	−0.96 ± 0.03	−1.13 ± 0.10	−1.51 ± 0.12	−1.31 ± 0.09
050712	–	0.10 ± 0.64	−1.25 ± 0.62	−1.01 ± 1.37	−0.30 ± 0.16	−0.64 ± 0.11	−2.89 ± 0.33	−0.63 ± 0.26	−1.11 ± 0.06
050726	–	−2.67 ± 0.80	−0.71 ± 3.69	–	–	−0.17 ± 0.14	−0.42 ± 0.67	–	–
050730	3.97[c]	0.16 ± 0.51	−0.27 ± 0.88	−0.90 ± 0.27	−2.17 ± 0.99	−1.10 ± 0.08	−1.31 ± 0.12	−1.00 ± 0.06	−2.67 ± 0.06
050801	1.38*	−0.50 ± 0.06	−0.90 ± 0.21	−0.69 ± 0.26	–	−0.37 ± 0.21	−1.78 ± 0.69	−1.34 ± 0.20	–
050802	1.71[d]	−0.09 ± 0.46	−0.68 ± 0.10	−0.60 ± 0.06	−0.81 ± 0.06	0.75 ± 0.28	−0.70 ± 0.09	−1.11 ± 0.04	−1.42 ± 0.06
050922c	2.198[e]	−1.02 ± 0.05	−0.60 ± 0.32	−1.04 ± 0.07	−1.12 ± 0.12	−0.85 ± 0.05	−0.92 ± 0.71	−1.17 ± 0.10	−1.48 ± 0.17
051109a	2.346[f]	−0.52 ± 0.44	–	−0.54 ± 0.12	−0.67 ± 0.07	−2.80 ± 0.30	–	−1.10 ± 0.05	−1.32 ± 0.03
060206	4.04795[g]	−1.89 - 2.18	–	−1.15 ± 0.17	−1.18 ± 0.09	1.14 ± 2.36	–	−0.95 ± 0.10	−1.36 ± 0.04
060223a	4.41[h]	−0.77 ± 0.68	−0.40 ± 0.59	–	–	−0.14 ± 0.26	4.76 ± 0.01	–	–
060418	1.4901[i]	0.01 ± 0.03	−1.39 ± 0.10	−1.34 ± 0.09	–	−3.21 ± 0.03	−0.94 ± 0.19	−2.29 ± 0.22	–
060512	0.4428[j]	−0.74 ± 0.08	–	−0.82 ± 0.11	−1.53 ± 0.34	−1.45 ± 0.11	–	−1.21 ± 0.17	−1.02 ± 0.23
060526	3.221[k]	−0.31 ± 0.08	−0.20 ± 0.13	−0.66 ± 0.75	–	1.41 ± 0.04	−3.35 ± 0.16	0.52 − 0.71	–
060605	3.8[l]	0.24 ± 0.13	–	−0.86 ± 0.15	–	−1.42 ± 0.24	–	−1.37 ± 0.09	–
060607a	3.082[m]	0.38 ± 0.02	−1.31 ± 0.06	−1.18 ± 0.18	–	−0.87 ± 0.02	−0.60 ± 0.07	−1.59 ± 0.07	–
060708	1.92*	−0.02 ± 0.11	–	−0.75 ± 0.06	−0.98 ± 0.09	−3.78 ± 0.10	–	−0.80 ± 0.07	−1.28 ± 0.06
060804	–	−0.72 ± 0.16	1.70 ± 2.57	−0.26 ± 0.24	−0.33 ± 0.15	0.39 ± 0.25	−3.77 ± 1.34	−1.50 ± 0.19	−0.86 ± 0.21
060908	2.43[n]	−1.19 ± 0.05	−1.16 ± 0.17	−2.18 ± 0.96	−0.53 ± 0.37	−0.63 ± 0.11	−1.07 ± 0.28	1.26 − 1.19	−1.12 ± 0.19
060912	0.937[o]	−0.98 ± 0.09	−1.01 ± 0.18	−0.59 ± 0.28	−0.75 ± 0.18	−0.74 ± 0.23	−1.10 ± 0.18	−1.27 ± 0.18	−1.03 ± 0.19
061007	1.262[p]	−1.69 ± 0.11	−1.70 ± 0.02	−1.48 ± 0.03	–	−1.83 ± 0.10	−1.55 ± 0.02	−1.75 ± 0.05	–
061021	0.77*	−0.93 ± 0.06	–	−0.58 ± 0.05	−1.24 ± 0.03	−1.83 ± 0.05	–	−0.99 ± 0.05	−1.13 ± 0.01
061121	1.314[q]	−0.12 ± 0.05	−0.80 ± 0.12	−0.48 ± 0.09	−0.32 ± 0.08	−3.90 ± 0.04	−0.40 ± 0.05	−0.99 ± 0.05	−1.56 ± 0.03
070318	0.836[r]	0.42 ± 0.03	−0.96 ± 0.03	−1.26 ± 0.08	−0.78 ± 0.03	−0.23 ± 0.03	−1.31 ± 0.11	−0.92 ± 0.10	−1.08 ± 0.04
070420	3.01*	0.72 ± 0.14	−1.94 ± 0.18	−1.25 ± 1.35	–	−4.38 ± 0.12	−0.23 ± 0.10	−1.24 ± 0.09	–
070529	2.4996[s]	−1.67 ± 0.14	0.07 ± 0.57	−0.22 ± 1.79	−0.62 ± 0.30	−1.54 ± 0.23	−1.02 ± 0.32	−0.82 ± 0.60	−0.96 ± 0.20

References: [a]Jakobsson et al. (2006c); [b]Foley et al. (2005); [c]Chen et al. (2005); [d]Fynbo et al. (2005); [e]Jakobsson et al. (2006c); [f]Quimby et al. (2005); [g]Fynbo et al. (2006); [h]Berger et al. (2006); [i]Prochaska et al. (2006); [j]Bloom et al. (2006); [k]Jakobsson et al. (2006c); [l]Peterson & Schmidt (2006); [m]Ledoux et al. (2006); [n]Rol et al. (2006); [o]Jakobsson et al. (2006a); [p]Jakobsson et al. (2006b); [q]Bloom, Perley & Chen (2006); [r]Jaunsen et al. (2007); [s]Berger, Fox & Cucchiara (2007).

optical/UV and X-ray light curves for multiple epochs, such that

$$\mathrm{rms} = \sqrt{\frac{\sum (\log C_{\mathrm{O}} - \log C_{\mathrm{X}})^2}{N}}, \quad (2)$$

where N is the number of data points. For each GRB, the rms deviation was calculated using a time window 1 dex (a factor of 10) wide shifted in steps of 0.15 in log time, starting from 10 s until the end of the observations. The section of X-ray light curve within each window was normalized to the corresponding section of optical/UV light curve. This was done by adding a constant term to the logarithmic X-ray light curve that minimized the χ^2 between the logarithmic optical/UV and logarithmic X-ray light curves. Rms deviation values close to zero indicate that the optical/UV and X-ray light curves behave the same, values larger than zero indicate that the light curves do not track each other precisely.

The starting time of 10 s and the movement of the window by 0.15 in log time ensures that we are performing the analysis systematically and that we can directly compare values of the rms deviation between two or more GRBs since the rms deviations have been determined from data in the same time ranges. The size of the window implies that the value of the rms deviation will only change when there is large scale temporal change in the light curve for instance flaring behaviour or changes in the temporal index of the X-ray and/or optical/UV light curves. There are rms deviation values which were determined across periods when an observing gap occurs, typically between 1000 and 3000 s, because the window over which we determine the rms deviation is larger than the observing gap.

The errors were determined using

$$\mathrm{rms}_{\mathrm{error}} = \sqrt{\frac{\sum e_{\mathrm{X}}^2 + e_{\mathrm{O}}^2}{N}}. \quad (3)$$

Since converting the count rate into logarithmic count rate causes the error bars to be asymmetric, e_{X} is taken to be the average positive and negative errors of $\log C_{\mathrm{X}}$, and e_{O} is taken as the average positive and negative error of $\log C_{\mathrm{O}}$. The rms deviation and error is shown in the bottom pane of each panel in Fig. 1.

The rms deviation was also determined for each GRB at four different specific epochs: (a)–(d), which are <500, 500–2000, 2000–20000 and >20000 s, respectively, and are marked in Fig. 1. Histograms of the rms deviation for epochs (a)–(d) can be seen in Fig. 2. The first epoch was selected to end at 500 s because by this time the optical/UV afterglows have finished rising and the optical/UV light curves have been observed for at least 100 s (Oates et al. 2009). Furthermore, this epoch finishes after the first X-ray break in the X-ray light curve, which occurs typically between 200 and 400 s (Evans et al. 2009). The second epoch was selected to end at 2000 s because there is an observing gap between ∼1000 and ∼3000 s. The third epoch starting from 2000 s was chosen to be 1-dex wide and so ends at 20 000 s. From 20 000 s onwards, the signal-to-noise ratio of the data begins to worsen, particularly in the optical and

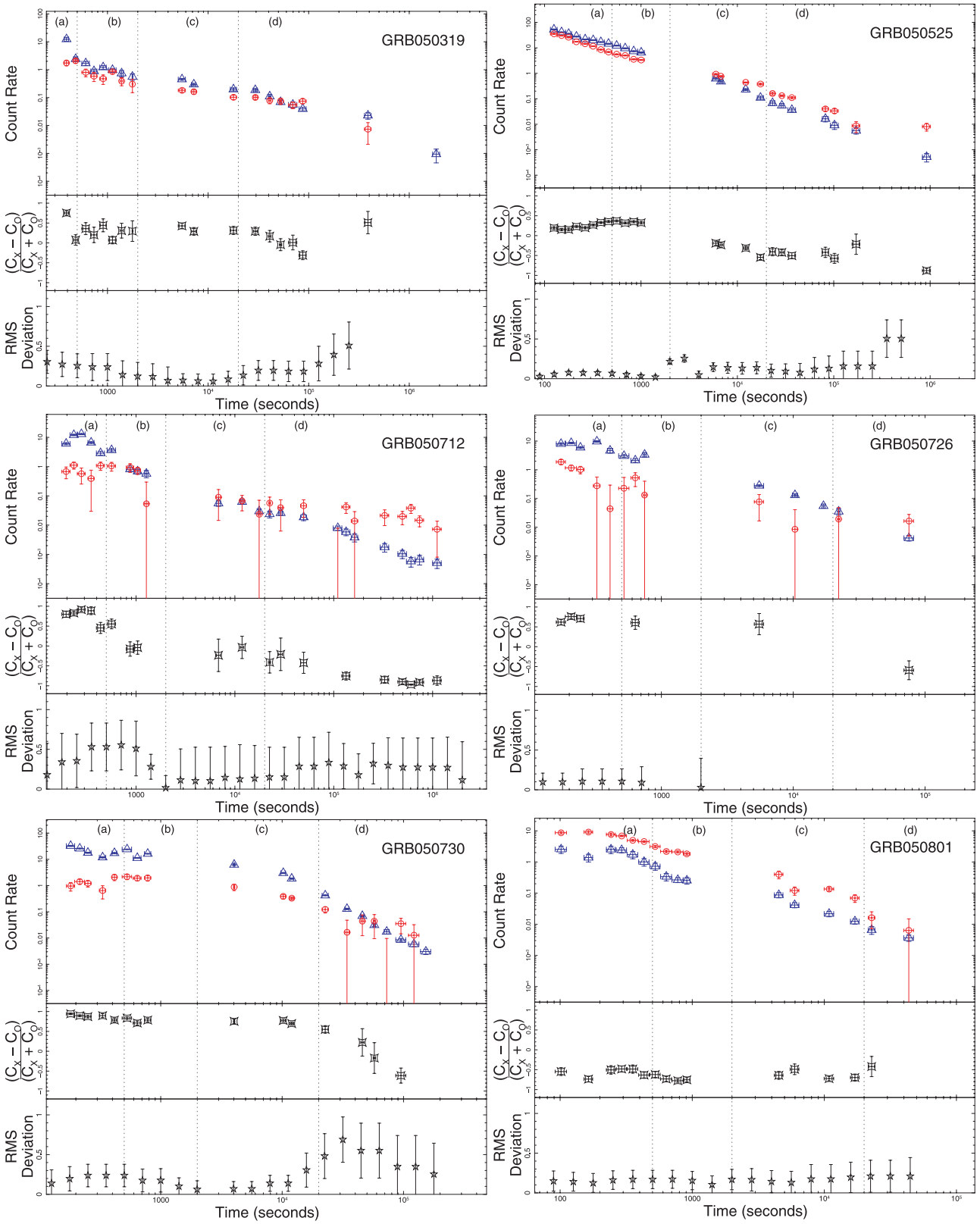

Figure 1. The 26 GRB X-ray and optical/UV afterglows. The dotted lines divide the light curves in to the epochs (a)–(d), which are <500, 500–2000, 2000–20 000 and >20 000 s, respectively. The top pane of each panel shows the X-ray and optical/UV (equivalent to v-band) light curves. The X-ray light curves (blue triangles) have been binned to have the same bin sizes as the optical/UV data (red circles). The middle pane of each panel shows the X-ray to optical/UV hardness ratio, given by hardness ratio $= (C_X - C_O)/(C_O + C_X)$, where C_O is the v-band count rate and C_X is the X-ray count rate. The bottom pane of each panel shows the rms deviation of the logarithmic X-ray light curves relative to the logarithmic, normalized optical/UV light curves in a time window 1-dex wide. The window was shifted in steps of 0.15 in log time and the rms deviation was calculated for each window.

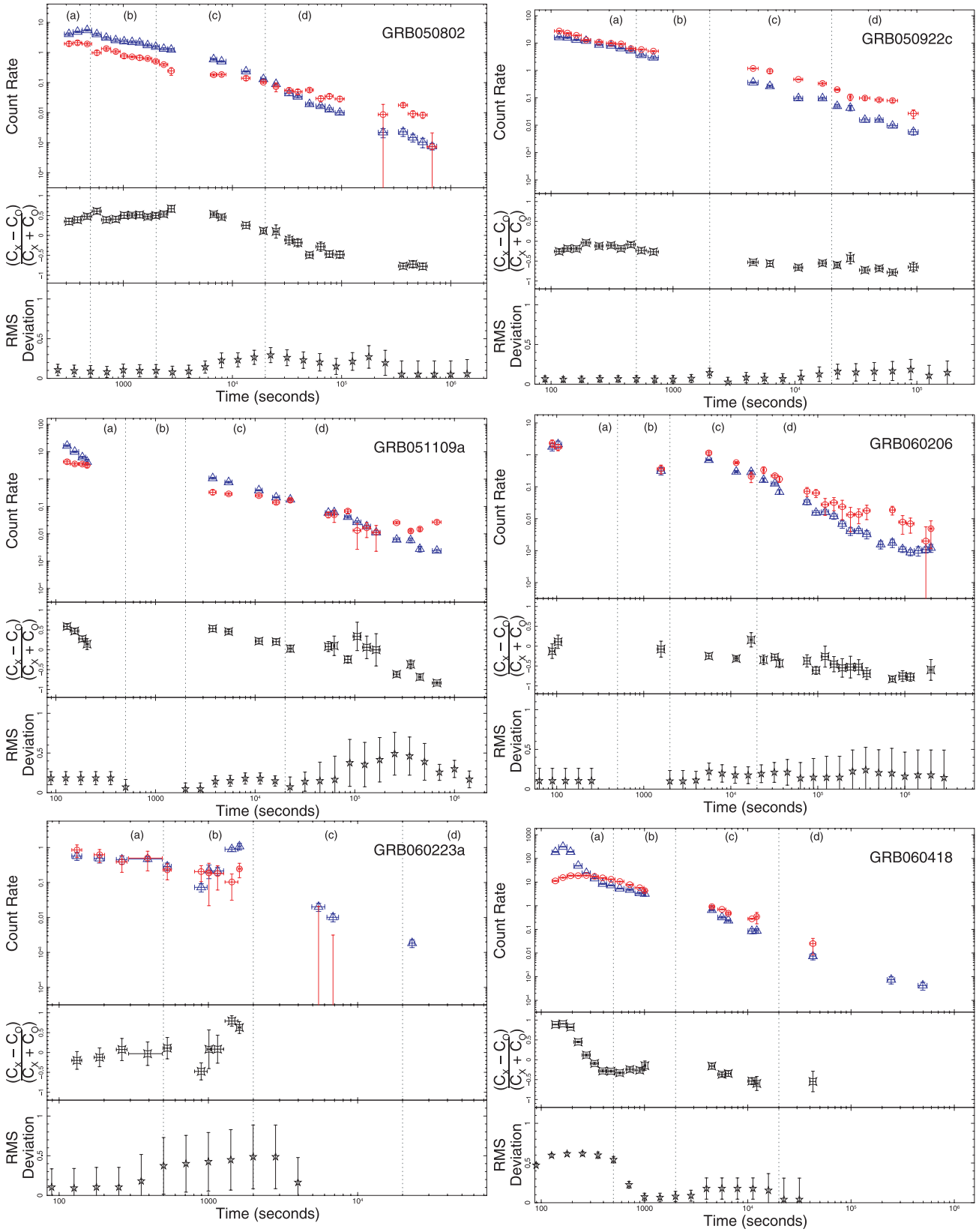

Figure 1 – *continued*

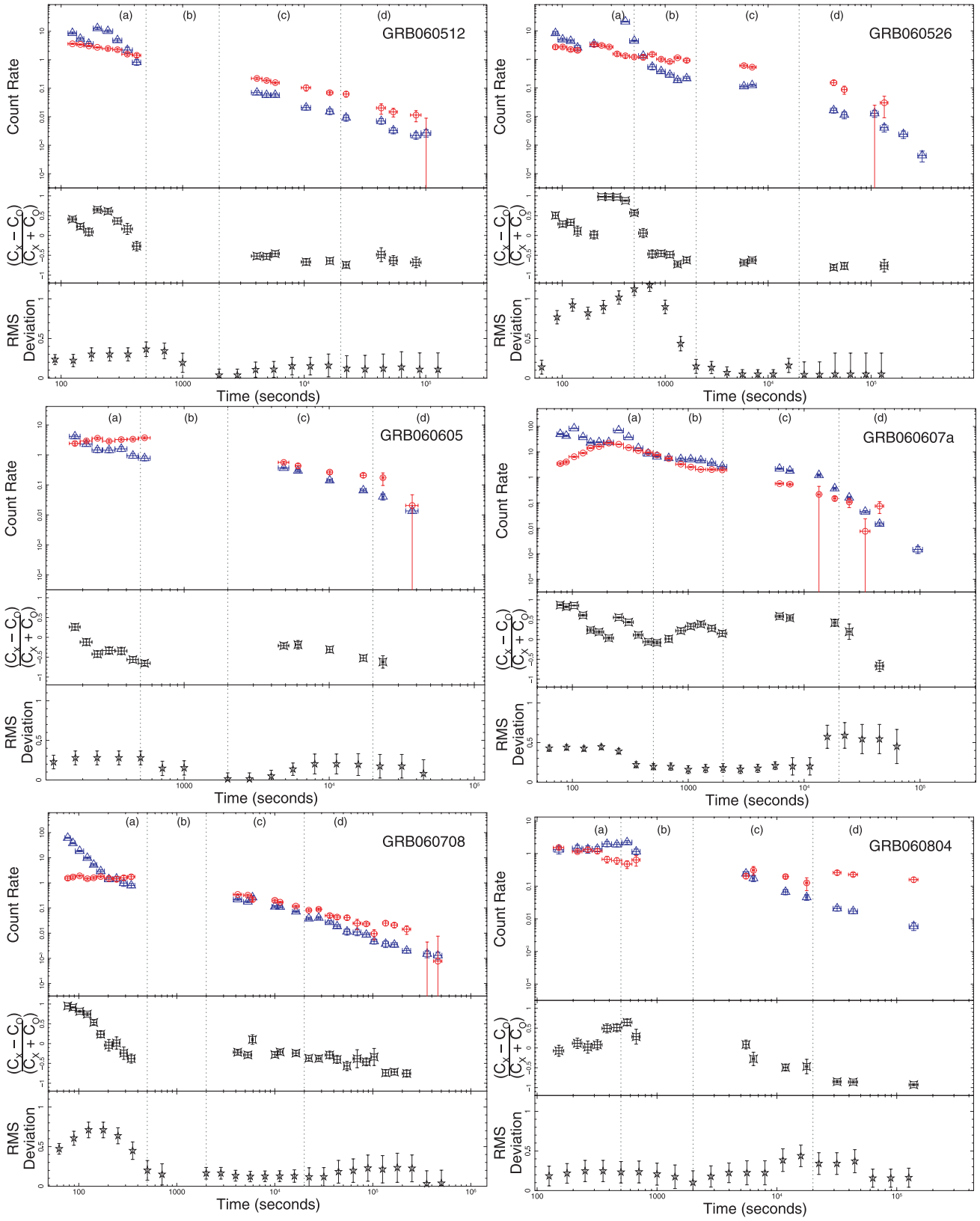

Figure 1 – *continued*

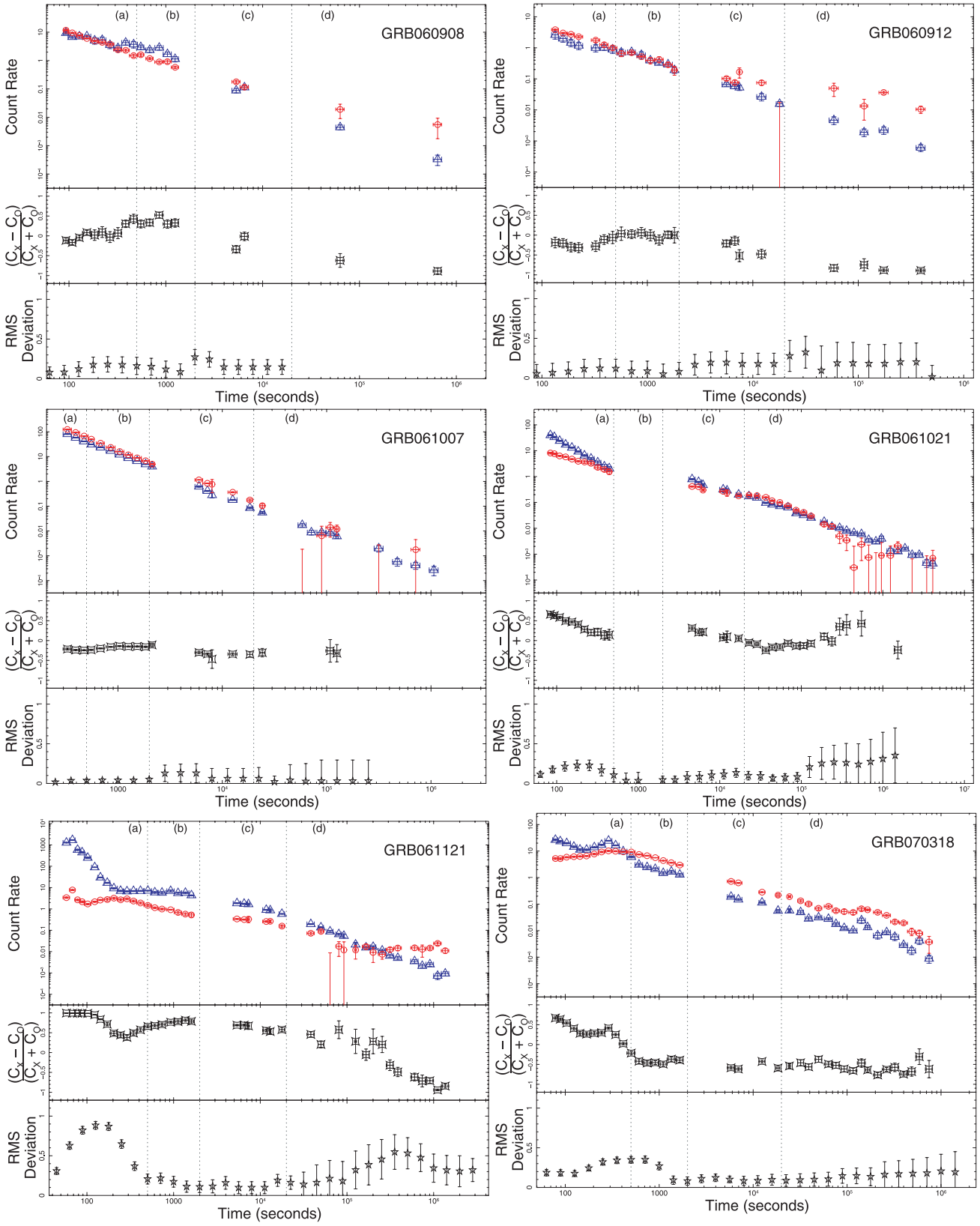

Figure 1 – *continued*

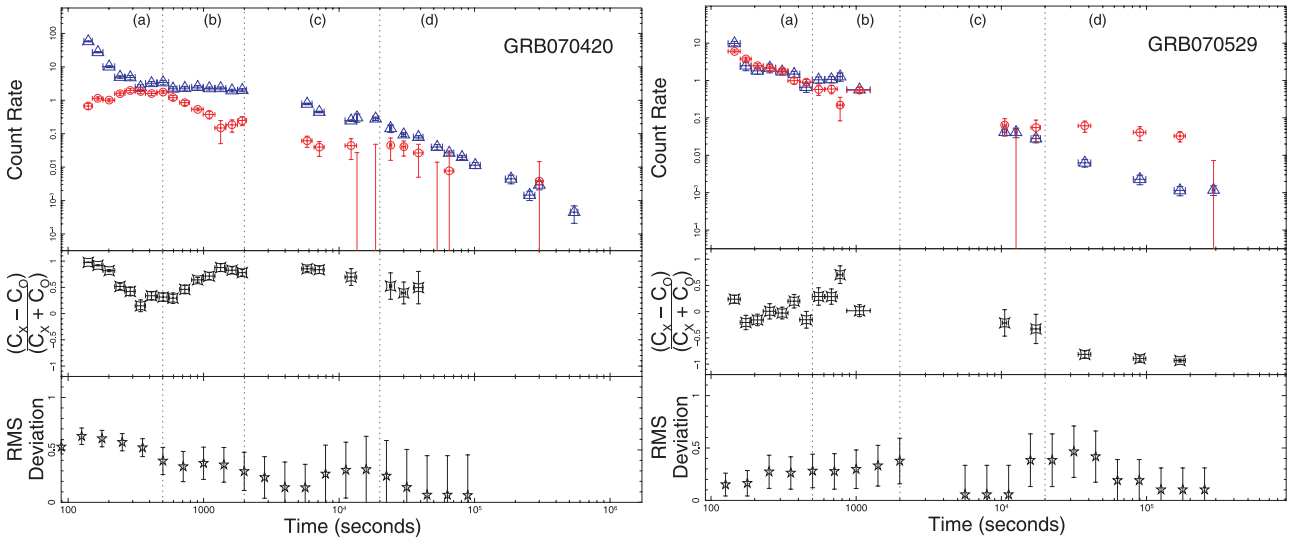

Figure 1 – *continued*

observations end, with some GRB observations ending as soon as $\sim 10^5$ s. We therefore took the fourth segment to be from 20000 s until the end of observations because a fifth segment would contain very few GRBs with few optical/UV and X-ray data points.

To allow systematic comparisons of the distribution of rms deviation with the temporal indices, these four epochs were also used when we measured the temporal indices of the light curves at multiple epochs. The determination of these values shall be described next.

2.3 Temporal indices

To determine how the overall behaviour of the optical/UV and X-ray light curves compare over the duration of the observations, we fit power laws individually to the optical/UV and X-ray data that lie within several successive epochs and compared the resulting values. The power laws were fitted to the data within the time frames: <500, 500–2000, 2000–20 000 and >20 000 s. The best-fitting values were determined using the IDL Levenberg–Marquardt least-squares fit routine supplied by Markwardt (2009). To ensure the power laws were constrained, the fits were only performed if there were at least two data points in both the optical/UV and X-ray light curves during the given epoch for which the signal-to-noise ratio was >1.

Since we are systematically comparing the behaviour of the optical/UV and X-ray light curves, we do not exclude the flaring behaviour because it is difficult to do this systematically. Instead we note that the temporal indices may be affected, particularly in the early afterglow, due to the presence of flares. Furthermore, as all data in each epoch are fit with a power law, if a break or a flare is present in that epoch the fit will determine a temporal index which corresponds to the overall evolution of the light curve, but which does not necessarily correspond to a genuine period of power-law decay. The optical/UV and X-ray temporal indices for all four epochs are given in Table 1. A comparison of the optical/UV and X-ray temporal indices for the four time frames are shown in Fig. 3. We have also determined the mean and intrinsic dispersion of the optical/UV and X-ray temporal indices for each epoch using the maximum likelihood method (Maccacaro et al. 1988), which assumes a Gaussian distribution. These values can be seen in Table 2.

3 RESULTS

The XRT and UVOT light curves are shown in Fig. 1. A preliminary examination shows that for the majority of GRBs, the optical/UV and X-ray light curves decay at similar rates overall. However, there are noticeable differences which tend to be observed at the beginning and tail ends of the light curves. For some GRBs (e.g. GRB 060708 and GRB 070318), during the early afterglow, the X-ray light curves decay more rapidly than the optical/UV and some of the optical/UV light curves rise. This behaviour tends to cease within a few hundred seconds, after which both the optical/UV and X-ray light curves decay at a similar rate. For a number of GRBs (e.g. GRB 050802 and GRB 060912), towards the end of observations the X-ray light curves appear to decay more quickly than the optical/UV light curves. Another noticeable feature is the presence of flares in the X-ray afterglows (e.g. GRB 060526 and GRB 060607a), which are not often observed in the optical/UV light curves and rarely at the same time as those observed in the X-ray light curves.

In the following three subsections, we describe the results of comparing the optical/UV and X-ray light curves using the three techniques outlined in Section 2. These three techniques provide information on the similarities between the optical/UV and X-ray afterglows in slightly different ways. The hardness ratio provides information on how the individual data points behave relative to each other and is a good indicator of temporal changes such as breaks in either band, flaring and rising behaviours. The rms deviation is a good indicator of how well the optical/UV and X-ray light curves track each other, and the temporal indices determined at the four epochs provide information on the average decay rates of the X-ray and optical/UV light curves during the four epochs (a)–(d) as defined in Section 2. Combining the information from these three techniques enables a comprehensive picture to be produced of the X-ray and optical/UV light curves using a systematic and statistical approach.

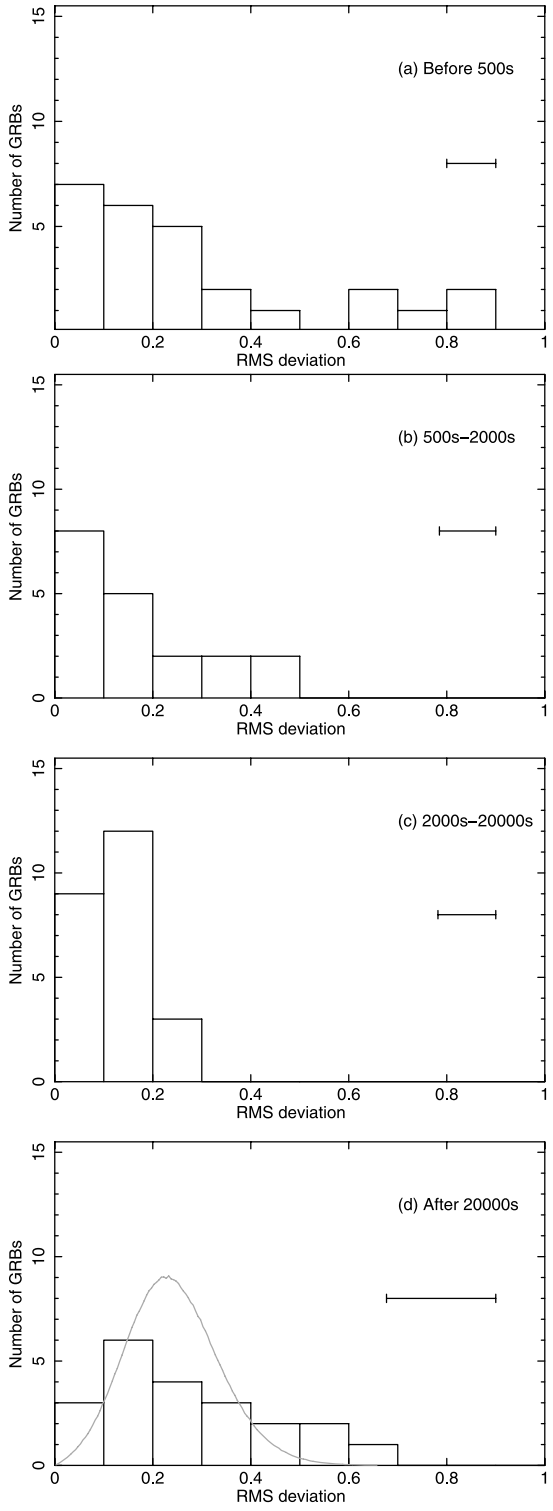

Figure 2. Distribution of rms deviation values determined from the normalized optical/UV and X-ray logarithmic light curves during four epochs: <500, 500–2000, 2000–20 000 and >20 000 s. The error bar in the top right corner represents the average error of the rms deviation in that particular epoch. In panel (d), the histogram shows the distribution of rms values determined from the normalized optical/UV and X-ray logarithmic light curves, while the grey line shows the normalized distribution of the rms deviation values from panel (c) convolved with the mean error from panel (d), see Section 3.2 for details.

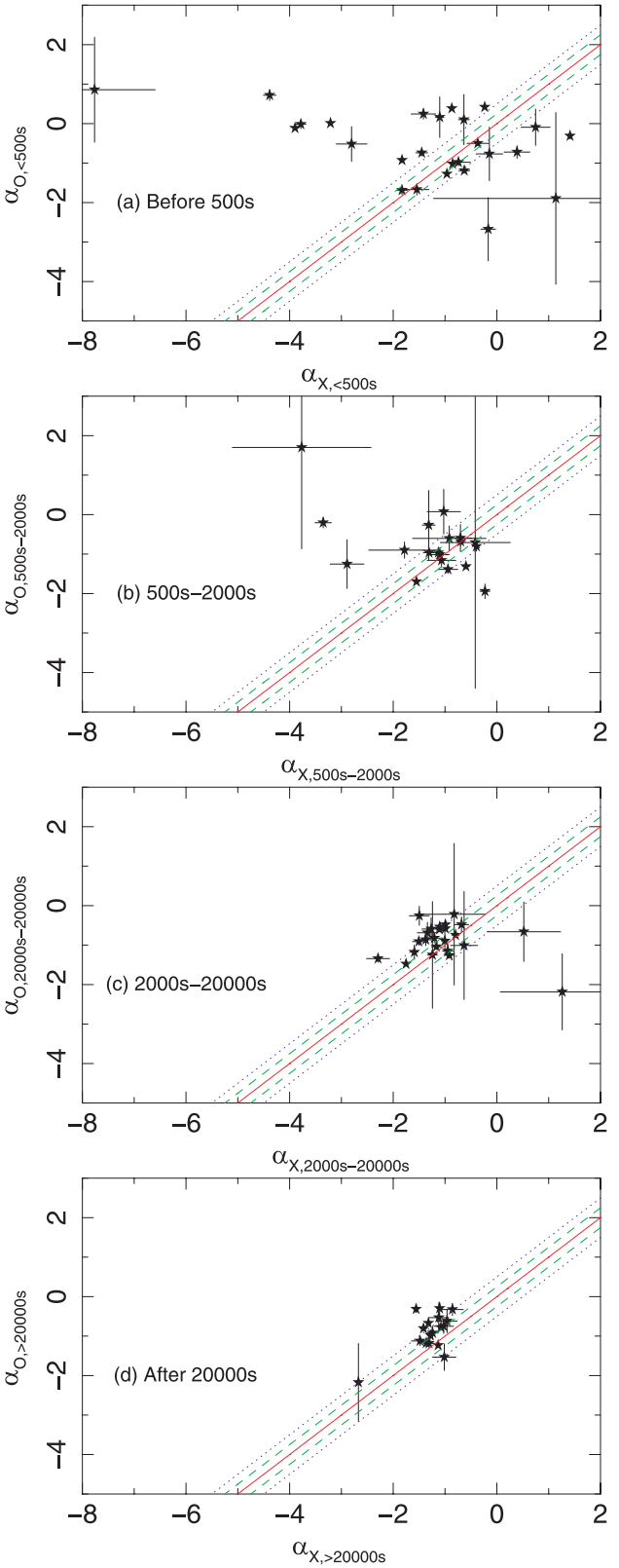

Figure 3. X-ray and optical/UV temporal indices determined from the light curves during four epochs: <500, 500–2000, 2000–20 000 and >20 000 s. The red solid line indicates where the optical/UV and X-ray temporal indices are equal. The green dashed lines indicate where $\alpha_O = \alpha_X \pm 0.25$ and the blue dotted lines represent $\alpha_O = \alpha_X \pm 0.50$.

Table 2. For the four epochs, this table provides the mean and intrinsic dispersion of the temporal indices of the X-ray and optical/UV light curves, and the mean and standard deviation of the rms deviations.

	Temporal index				rms deviation	
	Optical/UV		X-ray			
Time	Mean	Dispersion	Mean	Dispersion	Mean	Standard deviation
<500 s	$-0.51^{+0.17}_{-0.16}$	$0.67^{+0.19}_{-0.06}$	$-1.47^{+0.43}_{-0.32}$	$1.66^{+0.38}_{-0.15}$	0.29	0.25
500–2000 s	$-0.98^{+0.14}_{-0.16}$	$0.42^{+0.16}_{-0.06}$	$-0.97^{+0.45}_{-0.41}$	$1.60^{+0.42}_{-0.17}$	0.16	0.14
2000–20 000 s	$-0.88^{+0.11}_{-0.08}$	$0.30^{+0.10}_{-0.04}$	$-1.15^{+0.07}_{-0.12}$	$0.32^{+0.11}_{-0.04}$	0.12	0.05
>20 000 s	-0.84 ± 0.11	$0.31^{+0.11}_{-0.06}$	$-1.32^{+0.13}_{-0.11}$	$0.39^{+0.11}_{-0.05}$	0.27	0.17

3.1 X-ray to Optical/UV hardness ratio

The optical/UV to X-ray hardness ratios are shown in the middle panes of Fig. 1. These hardness ratios indicate relative spectral changes between the optical/UV and X-ray light curves, which could be due to the passage of a synchrotron frequency through an observed band, differences in the geometries of the emitting regions or due to additional or different emission mechanisms.

For the GRBs in this sample, the hardness ratios exhibit the most rapid variability during the first 1000 s, after which any changes tend to be more gradual. This corresponds to some of the optical/UV light curves rising, some of the X-ray light curves decaying steeply and X-ray flares (e.g. GRB 060418 and GRB 060526), which all typically occur within the first 1000 s. If none of these behaviours is observed within the first 1000 s, then the hardness ratio is observed to be fairly constant (e.g. GRB 050922c and GRB 061007). Periods of constant behaviour are an important indication that the X-ray and optical/UV light curves behave the same and that the production of emission during this period is intrinsically connected. After the first 1000 s, the hardness ratios vary more slowly and either are constant or slowly decrease. For some of the afterglows that have a constant hardness ratio, after a period, typically between $\sim$2000 and $\sim 10^5$ s, the hardness ratio begins to slowly decrease (e.g. GRB 050525 and GRB 050802). As we do not see the optical/UV light curves change to shallower decays around the same time as the X-ray to optical/UV hardness ratios decrease, this implies that the X-ray light curves decay more steeply than the optical/UV light curves during this period of hardness ratio decrease. From the hardness ratios alone the reason for the change in X-ray temporal index cannot be determined.

3.2 Rms deviation

The rms deviation of the optical/UV and X-ray light curves can be seen for each GRB in the bottom pane of each panel of Fig. 1. For most GRBs, there seems to be at least some period where the rms deviation is consistent with zero, indicating similar behaviour in the X-ray and optical/UV light curves for that period. For a few GRBs (e.g. GRB 050922c and GRB 061007), the rms deviation is consistent within errors with zero for almost their entire duration indicating that the X-ray and optical/UV track each other very well. Roughly half the GRBs have rms deviations, for at least half a dex, that are consistent within errors with having constant rms deviation, but at a value greater than zero, suggesting that the X-ray and optical/UV light curves behave consistently different (e.g. GRB 060607a and GRB 060804). If the light curves behave consistently different, this could indicate that the X-ray and optical/UV bands lie either side of a spectral frequency (see Section 4).

A notable period of rms deviation is before $\sim$1000 s, where for a number of GRBs the rms deviation is highly inconsistent with zero and varies rapidly (e.g. GRB 060418 and GRB 061121). This early period is where strong differences are observed in the behaviour of the optical/UV and X-ray light curves, which is reflected in their rms deviations. Other inconsistencies of the rms deviation from zero occur at around the same time as apparent changes in the temporal index in either the X-ray or optical/UV light curves. For instance GRB 050730 and GRB 050802 both have significant rms deviations at $\sim 3 \times 10^4$ s, around the time that the X-ray light curve changes decay rate.

Four histograms were produced using the rms deviation values determined for each GRB in the time intervals <500, 500–2000, 2000–20 000 and >20 000 s. The number of GRBs in each distribution are 26, 19, 24 and 21, for the four epochs, respectively. These histograms are shown in Fig. 2, and the mean and standard deviation of the rms deviation distributions are given in Table 2. The histogram for <500 s is shown in panel (a). This panel has the widest rms deviation distribution of all the four panels. The majority of GRBs lie within 0.30, but a few produce a tail stretching to 0.90. The distribution narrows by the second panel, which shows the rms deviation values determined from the epoch 500–2000 s, and the GRBs typically have lower rms deviation values. This is also reflected in the lower values for the mean and standard deviation in Table 2. By 2000–20 000 s, shown in panel (c), the distribution is at its narrowest and the individual rms deviation values are the lowest of all the four epochs, which is also indicated in Table 2 by the lowest mean and smallest standard deviation. In panel (d), showing the distribution from >20 000 s, the range in rms deviation values widens. However, the errors on the rms deviation values are also significantly larger at >20 000 s, suggesting that the widening of the distribution could be due to the larger uncertainties on the data points at this time. To check this, we performed a Monte Carlo simulation of the distribution of the rms deviation values in panel (c) convolved with the mean error of panel (d). To achieve this, for each light curve contributing to panel (d), we perturbed the values of $\log C_{\rm O} - \log C_{\rm X}$ in the 2000–20 000 s epoch by random displacements drawn from a Gaussian distribution with sigma equal to the mean rms error of panel (d), and computed the resulting rms. This process was repeated 1×10^5 times for each light curve to produce the simulated distribution. The normalized, simulated distribution is shown for comparison with the real distribution in panel (d). A Kolmogorov–Smirnov (KS) test comparing the real and simulated distributions shown in panel (d) returns a null-hypothesis probability of 28 per cent, implying that the distribution in panel (d) could intrinsically be the same distribution as in panel (c), but wider due to the larger uncertainty at later times.

3.3 Comparison of the X-ray and Optical/UV temporal indices

The optical/UV and X-ray temporal indices determined for the epochs: <500, 500–2000, 2000–20 000 and >20 000 s are shown

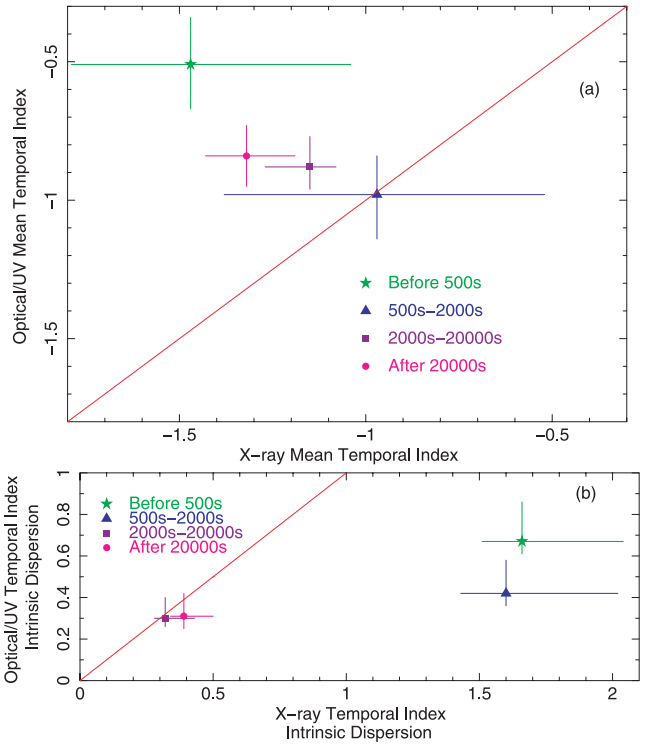

Figure 4. Panels (a) and (b) show the mean and intrinsic dispersion, respectively, of the X-ray and optical/UV temporal indices at four epochs. The red solid line in panel (a) represents the line of equal temporal index. The red solid line in panel (b) represents the line of equal intrinsic dispersion.

in panels (a)–(d) of Fig. 3. The individual panels contain 26, 20, 24 and 17 GRBs, respectively. In each panel of Fig. 3, the red solid line indicates where the optical/UV and X-ray temporal indices, $\alpha_{\rm O}$ and $\alpha_{\rm X}$ respectively, are equal. Points lying above the line decay more quickly in the X-ray than in the optical/UV, and the points below the line decay more quickly in the optical/UV than in the X-ray. The green dashed lines indicate where $\alpha_{\rm O} = \alpha_{\rm X} \pm 0.25$ and the blue dotted lines represent $\alpha_{\rm O} = \alpha_{\rm X} \pm 0.50$, where $\Delta\alpha = 0.25$ is expected if the synchrotron cooling frequency, $\nu_{\rm c}$, lies between the X-ray and optical/UV bands and $\Delta\alpha = 0.50$ is the maximum difference expected if $\nu_{\rm c}$ lies between the X-ray and optical/UV bands and the afterglow is experiencing energy injection. In panels (a) and (b) of Fig. 4, we show the X-ray and optical/UV means and intrinsic dispersions, respectively, for each of the four epochs. An initial examination of Figs 3 and 4 shows that the individual X-ray temporal indices change more than the optical/UV temporal indices over the four epochs. This indicates that the change from the scattered distribution of GRBs in the first panel of Fig. 3 to the clustering of the GRBs in the third and fourth panels of Fig. 3 is predominantly due to the change in the X-ray temporal indices.

For the first two epochs, shown in panels (a) and (b) of Fig. 3, the GRBs are not tightly clustered and appear to have a wide range of X-ray temporal indices, which is also seen in panel (b) of Fig. 4 as the large intrinsic dispersion in $\alpha_{\rm X}$ for the two epochs before 2000 s. In panels (a) and (b) of Fig. 3, there are approximately equal numbers of GRBs above and below the line of equal temporal index, implying that the optical/UV light curves for some GRBs decay faster than the X-ray light curves, while for other GRBs the X-ray light curves decay faster than the optical/UV light curves. A large fraction of GRBs in these two epochs have a difference of $\Delta\alpha > 0.5$ between the X-ray and optical/UV temporal indices implying large differences in the decay of the two bands and indicating that the difference is probably not due to the cooling frequency being positioned between the two bands. For the first epoch, shown in panel (a), there are four GRBs with rising X-ray light curves, indicated by a best-fitting temporal index of $\alpha_{\rm X,<500\,s} > 0$, and seven GRBs with rising optical/UV light curves indicated by a best-fitting temporal index of $\alpha_{\rm O,<500\,s} > 0$.

For the last two epochs, given in panels (c) and (d) of Fig. 3, the majority of the light curves are quite tightly clustered, implying that most of the GRB afterglows behave similarly at late times. The narrow range in temporal indices can also be observed in Fig. 4, by the small values of intrinsic dispersion of both the optical/UV and X-ray temporal indices. In both epochs, only a small number of GRBs have differences between optical/UV and X-ray temporal indices of $\Delta\alpha > 0.5$. More importantly, the majority of the GRBs in the last two epochs lie above the line of equal temporal index, implying that the optical/UV light curves decay more slowly than the X-ray light curves. One possible cause of a shallow decay in the optical/UV light curves would be a strong contribution from the host galaxy. If the host galaxy contribution was significant then at the tail end of the optical/UV light curve a constant count rate would be observed. However, for the majority of GRBs in this sample we do not observe a flattening at late times, implying that the optical/UV contribution from the host galaxy has a negligible effect on the light curve, and is not the reason why the optical/UV light curves decay on average less steeply compared with the X-ray light curves. The trend that the optical/UV light curves decay more slowly than the X-ray light curves is also indicated in Fig. 4, with the mean temporal indices for the epochs 2000–20 000 s and >20 000 s sitting above the line of equal temporal index. In fact even for the first two epochs, the mean values lie above or are consistent with lying above the line of equal temporal index, suggesting that X-ray light curves decay faster on average than optical/UV light curves throughout the entire observing period. Furthermore, for the epoch >20 000 s, shown in panel (d) of Fig. 3, the GRBs are clustered slightly to the left of those of the previous epoch 2000–20 000 s, shown in panel (c). This can also be seen in Fig. 4, with the X-ray mean for the >20 000 s at a slightly lower value than the 2000–20 000 s mean. This suggests that at least for some GRBs, there is a change in the X-ray temporal index to steeper values. This was also suggested in Section 3.1 from investigating the hardness ratios.

It is not possible, when investigating panels (c) and (d) of Fig. 3 individually, to determine how many light curves display a change in X-ray or optical/UV temporal index. Therefore, we have determined in Table 3 for the 17 GRBs in panel (d) the difference between the X-ray and optical/UV temporal indices determined at both the 2000–20 000 s and >20 000 s epochs. The table is coded by three symbols which divide the GRBs by temporal behaviour: both the X-ray and optical/UV temporal indices become more negative (triangles); the X-ray temporal index becomes more negative, but the optical/UV temporal index becomes more positive (squares) and the X-ray temporal index becomes more positive, but the optical/UV temporal index becomes more negative (circles). The first thing to note is that there are no GRBs whose X-ray and optical/UV light curves both become shallower in the >20 000 s epoch.

The most common behaviour, which occurs for nine of the 17 GRBs, is that both the best-fitting X-ray and optical/UV temporal indices become more negative i.e. both light curves become steeper. For the rest of the GRBs, four become steeper in the optical/UV, but shallower in the X-ray and four become steeper in the X-ray, while becoming shallower in the optical/UV. Examining the significance of the changes to these 17 GRBs, we find that seven GRBs, GRB

Table 3. Differences in temporal index from the 2000–20 000 s and 20 000 s onwards epochs. Symbols correspond to those in Fig. 5: ▲ both the X-ray and optical become steeper, ■ X-ray becomes steeper while the optical becomes shallower, ● X-ray becomes shallower while the optical becomes steeper.

GRB		$\Delta\alpha_X$	$\Delta\alpha_O$
GRB 050319	▲	-0.56 ± 0.18	-0.44 ± 0.26
GRB 050525	●	0.20 ± 0.15	-0.27 ± 0.12
GRB 050712	■	-0.47 ± 0.27	0.71 ± 1.38
GRB 050730	▲	-1.67 ± 0.09	-1.28 ± 1.02
GRB 050802	▲	-0.31 ± 0.07	-0.20 ± 0.09
GRB 050922c	▲	-0.32 ± 0.19	-0.08 ± 0.14
GRB 051109a	▲	-0.22 ± 0.06	-0.13 ± 0.14
GRB 060206	▲	-0.41 ± 0.11	-0.03 ± 0.19
GRB 060512	●	0.19 ± 0.28	-0.71 ± 0.36
GRB 060708	▲	-0.49 ± 0.09	-0.23 ± 0.11
GRB 060804	●	0.64 ± 0.29	-0.07 ± 0.29
GRB 060908	■	-2.38 ± 1.21	1.65 ± 1.03
GRB 060912	●	0.24 ± 0.26	-0.16 ± 0.34
GRB 061021	▲	-0.14 ± 0.05	-0.65 ± 0.05
GRB 061121	■	-0.56 ± 0.06	0.17 ± 0.12
GRB 070318	■	-0.16 ± 0.11	0.48 ± 0.08
GRB 070529	▲	-0.14 ± 0.63	-0.40 ± 1.82

050319, GRB 050730, GRB 051109a, GRB 060206, GRB 060804 GRB 060908 and GRB 061121, are consistent with no change in the optical/UV temporal index, while the X-ray is inconsistent at $\geq 2\sigma$, indicating a break. The hardness ratios of these GRBs provide evidence that the breaks are chromatic because the hardness ratios soften for these GRBs during the last two epochs (see also Section 3.1). GRBs, GRB 050525, GRB 060512 and GRB 070318, have X-ray temporal indices that are consistent with no change, while the optical/UV temporal index between the two epochs is not consistent with being the same at $\geq 2\sigma$, which suggests a chromatic break. However, the hardness ratio of GRB 050525 does not show an obvious hardening, which would be expected if a break was observed in the optical and not the X-ray, but it does soften in the 2000–20 000 s epoch and becomes constant during the >20 000 s epoch. The hardness ratios for GRB 060512 and GRB 070318 appear to be constant during the last two epochs, implying that there is not a break in the optical/UV. GRBs, GRB 050712, GRB 050922c, GRB 060912 and GRB 070529, are consistent with no change in either the X-ray or the optical/UV and the remaining three GRBs have optical/UV and X-ray temporal indices that are different between the two epochs at $\geq 2\sigma$, suggesting a change in temporal index in both light curves.

The other interesting behaviour, shown in Fig. 5, is that a small number of GRBs appear to cross the line of equal temporal index, but this is only significant for two GRBs, GRB 070318, GRB 061021. These GRBs have one data point more than 2σ above the line and the other data point more than 2σ below the line of equal temporal index, which can be seen in the inset panel of Fig. 5. For all other GRBs, at least one of their data points is consistent within 2σ lying on either side of the line of equal temporal index. GRB 061021 is consistent with crossing from above to below the line of equal temporal index, indicating that a change from the optical/UV light curve having a shallower decay than the X-ray to the X-ray light curve having a shallower decay than the optical/UV. This is also observed in the hardness ratio for this GRB, which softens during the 2000–20 000 s epoch, indicating that the X-ray decays more

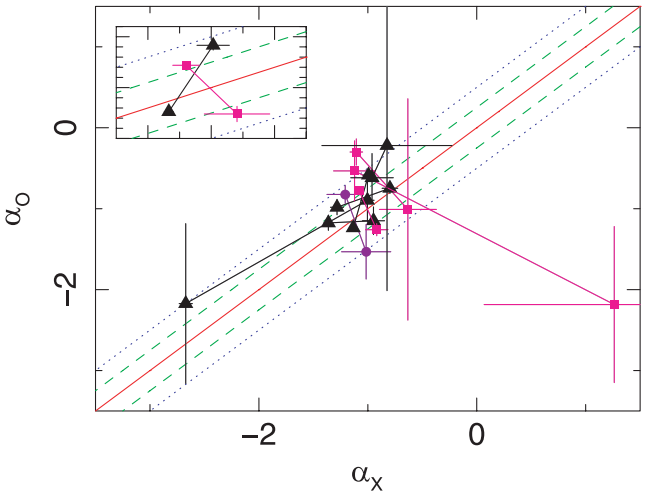

Figure 5. This figure plots the X-ray and optical/UV temporal indices determined from the epochs 2000–20 000 and >20 000 s for eight GRBs, which appear to cross the line of equal temporal index. Each GRB has a pair of data points linked together which show the temporal indices in the 2000–20 000 and >20 000 s epochs. The symbols, which correspond to those in Table 3, show how the temporal index changes between the two epochs. Pairs of black triangles are those GRBs for which the X-ray and optical/UV temporal indices become more negative between the epochs 2000–20 000 and >20 000 s (i.e. they move down and to the right). Pairs of purple circles are those GRBs in which the X-ray temporal index becomes less negative and the optical/UV temporal index becomes more negative (i.e. they move down and to the left) and the pairs of pink squares are GRBs for which the X-ray temporal index becomes more negative and the optical/UV temporal index becomes less negative (i.e. they move up and to the right). The red solid line indicates where the optical/UV and X-ray temporal indices are equal, the green dashed line indicates where $\alpha_O = \alpha_X \pm 0.25$ and the blue dotted lines represents $\alpha_O = \alpha_X \pm 0.50$. The inserted panel shows the two GRBs, GRB 070318 and GRB 061021, which are consistent with having one data point more than 2σ above the line of equal temporal index and the other data point more than 2σ below the line of equal temporal index.

steeply than the optical/UV, but hardens during the >20 000 s epoch indicating that the optical/UV light curve decays more rapidly than the X-ray. As for the other GRB, GRB 070318, this GRB is consistent with crossing from below to above the line of equal temporal index, indicating a change from the X-ray light curve having a shallower decay than the optical/UV to the optical/UV light curve having a shallower decay than the X-ray. A subtle softening of the hardness ratio for GRB 070318 implies that the X-ray light curve in the >20 000 s epoch decays more quickly than the optical/UV.

From Table 3 and Fig. 5, we can draw three significant conclusions: seven of the 17 (∼41 per cent) afterglows have a break, which is observed only in the X-ray light curve between 2000 s and the end of observations; there are no afterglows that becomes shallower in the optical/UV and in the X-ray; two GRBs traverse the line of equal temporal index, one from above to below the line of equal temporal index and the other from below to above the line of equal temporal index.

4 DISCUSSION

All three analysis methods indicate that the X-ray and optical/UV light curves behave most differently before 500 s. The rms deviation distribution and the mean temporal indices together indicate that the optical/UV and X-ray light curves behave most similarly during the 2000–20 000 s epoch. For all four epochs, we find that

the optical/UV light curves decay more slowly on average than the X-ray. We also find through investigation of the temporal indices and the hardness ratios that chromatic breaks are observed in some of the GRB afterglows, with the breaks observed in the X-ray light curves.

In the following sections we shall examine two models, a single component jet and a jet with additional emission regions such as a two component jet, or late 'prompt' emission, to determine whether either of these models can explain the observations.

4.1 Single component outflow

The temporal indices expected from a synchrotron dominated outflow are determined by a set of equations (Sari, Piran & Narayan 1998; Meszaros, Rees & Wijers 1998; Sari, Piran & Halpern 1999; Chevalier & Li 2000; Dai & Cheng 2001; Racusin et al. 2009, see last reference for a comprehensive list). These are mathematical expressions that relate the temporal index to predominantly a microphysical parameter, a physical parameter and the positioning of two spectral frequencies relative to the observed band. Specifically, these are the electron energy index p, which is typically between 2 and 3 (Panaitescu & Kumar 2002; Starling et al. 2008; Curran et al. 2010), the density profile of the external medium (constant or wind like) and the relative positions in the spectrum of the synchrotron frequencies, primarily the synchrotron cooling frequency ν_c and the synchrotron peak frequency ν_m (see Table 4). There is a third synchrotron frequency, the synchrotron self-absorption frequency, but this frequency does not influence the optical/UV or the X-rays during the time-scales studied here. Recent observations of *Swift* GRB afterglows have shown that, in some cases, the temporal indices are shallower than expected (Nousek et al. 2006). This led to the hypothesis that, at least for a certain time, the ejecta may be injected with some additional energy (see Zhang et al. 2006, for a discussion and for other possible interpretations). The temporal indices of these GRBs should then be satisfied by the energy injected temporal relations (see Table 4). The amount of energy injection is measured by the luminosity index, q, which varies between 0 and 1 in the luminosity relation $L(t) = L_0(t/t_0)^{-q}$, where t is the observers time, t_0 is the characteristic time-scale for the formation of a self-similar solution, which is roughly equal to the time at which the external shock starts to decelerate (Zhang & Mészáros 2001). When $q = 1$ the injected temporal relations reduce to the non-injected closure relations.

The position of the synchrotron cooling frequency relative to the synchrotron peak frequency dictates whether electrons are in a slow cooling ($\nu_m < \nu_c$) or fast cooling regime ($\nu_c < \nu_m$). The fast cooling closure relations provided in Table 4 are valid only in the adiabatic regime and are not valid for radiative evolution (Sari et al. 1998). For a single component jet, it is expected that the optical/UV and X-ray emission are produced within the same region and therefore are explained by the same synchrotron spectrum, with the possibility that one or more of the synchrotron frequencies are between these two observing bands. This means that the optical/UV and X-ray temporal indices, determined from an afterglow, should be described

Table 4. This table provides the ranges in temporal index for the temporal relations that are expected from synchrotron emission with and without energy injection (Zhang & Mészáros 2004; Zhang et al. 2006). The electron energy index p dictates the range of values of the temporal index for each temporal relation. The electron energy index p and the luminosity index q dictate the range of values of the temporal index for each temporal relation. When $q = 1$ the energy injected temporal relations reduce to those of the non-injected cases. The temporal relations for the jet case can be found in Panaitescu et al. (2006).

	Temporal relations		$p = 2$		$p = 3$	
	Non-injected ($q = 1$)	Energy injected ($0 \leq q < 1$)	$q = 0$ α	$q = 1$ α	$q = 0$ α	$q = 1$ α
ISM slow cooling						
$\nu < \nu_m$	$1/2$	$(8 - 5q)/6$	1.33	0.50	1.33	0.50
$\nu_m < \nu < \nu_c$	$3(1 - p)/4$	$\frac{(6-2p)-(p+3)q}{4}$	0.5	−0.75	0.00	−1.50
$\nu > \nu_c$	$(2 - 3p)/4$	$\frac{(4-2p)-(p+2)q}{4}$	0.00	−1.00	−0.50	−1.75
ISM fast cooling						
$\nu < \nu_c$	$1/6$	$(8 - 7q)/6$	1.33	0.17	1.33	0.17
$\nu_c < \nu < \nu_m$	$-1/4$	$(2 - 3q)/4$	0.50	−0.25	0.50	−0.25
$\nu > \nu_m$	$(2 - 3p)/4$	$\frac{(4-2p)-(p+2)q}{4}$	0.00	−1.00	−0.50	−1.75
Wind slow cooling						
$\nu_< \nu_m$	0	$(1 - q)/3$	0.33	0.00	0.33	0.00
$\nu_m < \nu < \nu_c$	$(1 - 3p)/4$	$\frac{(2-2p)-(p+1)q}{4}$	0.00	−1.25	−1.00	−2.00
$\nu > \nu_c$	$(2 - 3p)/4$	$\frac{(4-2p)-(p+2)q}{4}$	0.00	−1.00	−0.50	−1.75
Wind fast cooling						
$\nu < \nu_c$	$-2/3$	$-(1 + q)/3$	−0.33	−0.67	−0.33	−0.67
$\nu_c < \nu < \nu_m$	$-1/4$	$(2 - 3q)/4$	0.50	−0.25	0.50	−0.25
$\nu > \nu_m$	$(2 - 3p)/4$	$\frac{(4-2p)-(p+2)q}{4}$	0.00	−1.00	−0.50	−1.75
Jet slow cooling						
$\nu < \nu_m$	$-1/3$	–	–	−0.33	–	−0.33
$\nu_m < \nu < \nu_c$	$\sim -p$	–	–	−2.00	–	−3.00
$\nu > \nu_c$	$\sim -p$	–	–	−2.00	–	−3.00

by temporal relations which rely on the same assumptions about the external medium, the electron energy index, p, and the value of q.

In order to assess the validity of this scenario, we shall consider the mean X-ray and optical/UV temporal indices and search for a common set of closure relations that are allowed in all the four temporal epochs, and we shall use the hardness ratios and the rms deviations to support and confirm our findings. To determine if a scenario is acceptable, consistent values of p must be derived from the mean temporal indices of the optical/UV and X-ray light curves at the different epochs. As we are using the average properties of the sample, we note that the conclusion drawn is typical of the sample, but should not be taken as the conclusive explanation for individual GRBs, which should be investigated individually.

4.1.1 Implications of the mean GRB temporal properties

Before 500 s, the mean temporal indices of the X-ray and optical/UV afterglows are $\alpha_{\mathrm{X},<500\,\mathrm{s}} = -1.47^{+0.43}_{-0.32}$ and $\alpha_{\mathrm{O},<500\,\mathrm{s}} = -0.51^{+0.17}_{-0.16}$. The X-ray mean temporal index can be explained by several of the non-injected temporal relations in Table 4, and the optical/UV mean temporal index can be explained either in a scenario with $\nu < \nu_{\mathrm{c}}$, a wind medium and fast cooling electrons (which would be contrived as the theoretical temporal index for this scenario is a single distinct value while in reality the optical/UV light curves, before 500 s have a range in temporal index), or by several of the energy injected temporal relations. The lack of discrimination of the temporal expressions for the light curves before 500 s is not unexpected as there is a wide range in temporal behaviour in both the optical/UV and the X-ray. The wide temporal behaviour is also observed in the rms deviation histogram as a wide distribution during this epoch.

Moving to the next epoch between 500 and 2000 s, the mean temporal indices of the X-ray and optical/UV light curves are $\alpha_{\mathrm{O},500-2000\,\mathrm{s}} = -0.98^{+0.16}_{-0.14}$ and $\alpha_{\mathrm{X},500-2000\,\mathrm{s}} = -0.97^{+0.45}_{-0.41}$. Both are consistent with the non-injected temporal relations for a slow cooling interstellar medium (ISM)-like medium with $\nu_{\mathrm{m}} < \nu < \nu_{\mathrm{c}}$. This gives two values of p, $p = 2.30^{+0.16}_{-0.14}$ from the optical/UV and $p = 2.29^{+0.45}_{-0.41}$ from the X-ray, which are consistent to within 1σ. However, both the X-ray and optical/UV mean temporal indices could also be reproduced by the relations for both the ISM-like and wind-like media in the slow cooling case $\nu > \nu_{\mathrm{c}}$ and in the fast cooling case $\nu > \nu_{\mathrm{m}}$ giving values $p = 1.97^{+0.16}_{-0.14}$ for the optical/UV and $1.96^{+0.45}_{-0.41}$ for the X-ray, which again are consistent to within 1σ. Furthermore, there is one more option: with slow cooling electrons in an ISM-like medium, the values of the temporal indices allow the possibility that $\nu_{\mathrm{m}} < \nu_{\mathrm{O}} < \nu_{\mathrm{c}} < \nu_{\mathrm{X}}$, which produces values of $p = 2.29^{+0.45}_{-0.41}$ for the X-ray and $p = 1.97^{+0.16}_{-0.14}$ from the optical/UV, which are consistent to within 1σ. The temporal indices can also be explained by the energy injected relations, in these cases the values of p may change depending upon the energy injection parameter q. If energy injection is considered then the temporal relations for a wind-like medium are also acceptable for slow cooling with either $\nu_{\mathrm{m}} < \nu_{\mathrm{O}} < \nu_{\mathrm{X}} < \nu_{\mathrm{c}}$ or $\nu_{\mathrm{m}} < \nu_{\mathrm{O}} < \nu_{\mathrm{c}} < \nu_{\mathrm{X}}$ and for fast cooling with $<\nu_{\mathrm{c}} < \nu_{\mathrm{m}} < \nu_{\mathrm{O}} < \nu_{\mathrm{X}}$. The narrower rms distribution histogram compared to the previous epoch indicates that the optical/UV and X-ray light curves for a large fraction of GRBs behave in a similar way, consistent with the expectations of a single synchrotron spectrum producing both light curves.

During the epoch 2000–20 000 s, the mean X-ray temporal index is $\alpha_{\mathrm{X},2000\,\mathrm{s}-20\,000\,\mathrm{s}} = -1.15^{+0.07}_{-0.12}$ and the mean optical/UV temporal index is $\alpha_{\mathrm{O},2000\,\mathrm{s}-20\,000\,\mathrm{s}} = -0.88^{+0.11}_{-0.08}$. The difference in α between the optical/UV and X-ray indices, $\Delta\alpha = 0.27^{+0.16}_{-0.10}$, implies that the optical/UV and X-ray do not lie on the same spectral segment. This difference is consistent with a cooling break ($\Delta\alpha = 0.25$) lying in between the X-ray and optical/UV bands. The only non-energy injected temporal relations that can produce both mean values are the ISM slow cooling temporal relations for the case $\nu_{\mathrm{m}} < \nu_{\mathrm{O}} < \nu_{\mathrm{c}} < \nu_{\mathrm{X}}$. These relations give consistent values of p: $p = 2.17^{+0.11}_{-0.08}$ determined using the optical/UV temporal mean and $p = 2.20^{+0.07}_{-0.12}$ determined with the X-ray temporal mean. Looking at the temporal values in Table 4, the only temporal relation for a wind-like medium that could explain wide ranges in both temporal indices and with the X-ray and optical/UV having different temporal indices would be for the slow cooling case with $\nu_{\mathrm{m}} < \nu_{\mathrm{O}} < \nu_{\mathrm{c}} < \nu_{\mathrm{X}}$. However, this cannot explain these temporal indices even with energy injection, since in the wind-medium (if $\nu_{\mathrm{c}} < \nu_{\mathrm{O}}$, ν_{X} in the fast cooling case or $\nu_{\mathrm{m}} < \nu_{\mathrm{O}}$, ν_{X} in the slow cooling case) the X-ray is required to be shallower than the optical/UV by 0.25, which is the opposite of what is observed. As there are only a small number of GRBs with a break in the optical/UV light curve (Oates et al. 2009), the temporal indices are consistent with an ISM-like medium with ν_{c} being between the X-ray and optical/UV bands during the 500–2000 and 2000–20 000 s epochs. This implies that we have slow cooling electrons in an ISM-like medium with $\nu_{\mathrm{m}} < \nu_{\mathrm{O}} < \nu_{\mathrm{c}} < \nu_{\mathrm{X}}$ from 500 to 20 000 s. The narrowness and the low values of the rms deviation histogram for the 2000–20 000 s epoch agree with a single synchrotron spectrum producing the X-ray and optical/UV emission for almost all GRBs during this epoch.

For the final epoch >20 000 s, the mean X-ray temporal index is $\alpha_{\mathrm{X},>20\,000\,\mathrm{s}} = -1.33^{+0.13}_{-0.11}$ and the mean optical/UV temporal index is $\alpha_{\mathrm{O},>20\,000\,\mathrm{s}} = -0.84 \pm 0.11$. Again the mean values can only be produced by the non-injected temporal relations for the ISM slow cooling regime with $\nu_{\mathrm{m}} < \nu_{\mathrm{O}} < \nu_{\mathrm{c}} < \nu_{\mathrm{X}}$. Wind-like density cannot explain the temporal indices of this epoch either since, similar to the previous epoch, the optical/UV and X-ray temporal indices have wide ranges, but the optical/UV is shallower than the X-ray, which cannot be explained by the temporal relations for a wind-like medium, even including energy injection. The values of p determined from the non-injected temporal relations for the ISM slow cooling regime with $\nu_{\mathrm{m}} < \nu_{\mathrm{O}} < \nu_{\mathrm{c}} < \nu_{\mathrm{X}}$ are $p = 2.12 \pm 0.11$ for the optical/UV and $p = 2.44^{+0.13}_{-0.11}$ for the X-ray. These values are marginally consistent with each other at 2σ. The p value determined from the optical/UV is consistent with p value determined from the optical/UV in the previous epoch. The p value determined from the X-ray is marginally consistent at 2σ with the p value derived from the mean X-ray temporal index from the same regime in the previous epochs. The large errors on the rms deviations determined for the >20 000 s epoch means that little can be implied from this >20 000 s rms deviation distribution.

The narrowness and the small valued rms deviation distribution in the 500–2000 and 2000–20 000 s epochs support the hypothesis of a single synchrotron emission spectrum from a single component emission region. The general consistency of the mean temporal indices with the non-injected temporal relations, producing consistent and realistic p values, suggests that at least from 500 s, the sample on average is consistent with slow cooling electrons in a constant density medium with $\nu_{\mathrm{m}} < \nu_{\mathrm{O}} < \nu_{\mathrm{c}} < \nu_{\mathrm{X}}$. The mean temporal indices of the last three epochs are consistent with a single component outflow, without the need for energy injection, although we cannot exclude the requirement of energy injection, which would complicate this simplistic picture and would increase the value of p. However, it is unlikely that this simple picture can explain all GRBs and we need to determine how this picture changes on a

GRB to GRB basis. Therefore, we shall compare this picture with the individual temporal indices at each epoch.

4.1.2 Implications of the individual GRB properties

In Fig. 3, in each panel the green dashed line represents the difference between the optical/UV and X-ray temporal indices $\Delta\alpha = 0.25$, expected when ν_c lies between these bands, and the blue dotted line represents the maximum difference $\Delta\alpha = 0.5$, expected when ν_c lies between these bands and the afterglow is energy-injected. Furthermore, $\alpha_X + 0.25 \leq \alpha_O \leq \alpha_X + 0.50$ is expected for a constant density medium, while $\alpha_X - 0.50 \leq \alpha_O \leq \alpha_X - 0.25$ is expected for a wind-like medium.

For the epoch <500 s, shown in panel (a) of Fig. 3, it is clear that the mean temporal indices are not representative of the full behaviour of the optical/UV and X-ray light curves. It is also clear from the rapid variability in the hardness ratios of individual GRBs and from the changes in rms deviations during this epoch that a simple outflow ploughing into a constant density medium is too simplistic. This is also shown in Fig. 3 by the lack of consistency with $\alpha_X \leq \alpha_O \leq \alpha_X + 0.50$. Instead, this figure shows a wide range in behaviour that physically can be divided into several groups.

(i) Five GRBs are consistent with $\alpha_O = \alpha_X - 0.25$, suggesting that these GRBs lie in a wind medium with a cooling break between the X-ray and optical/UV bands. The temporal range of these GRBs is $-1.54 < \alpha_{X,<500\,s} < -0.14$ and $-1.67 < \alpha_{O,<500\,s} < -0.50$. As the shallowest temporal index produced by a wind medium with $\nu_O < \nu_c < \nu_X$ is $\alpha_X = \alpha_O + 0.25 = -1.00$, this implies that for at least a couple of these GRBs energy injection is required.

(ii) Four GRBs have $0 < \alpha_{X,<500\,s}$. A visual inspection of these GRBs during this period reveals that three of these GRBs have flares in the X-ray emission that are not observed in the optical/UV, implying late-time central engine activity (Falcone et al. 2007). Furthermore, the three GRBs with X-ray flares all have optical/UV temporal indices $-0.80 < \alpha_{O,<500\,s} \lesssim 0.00$, which are too shallow to be explained by the non-energy injected temporal relations, therefore, implying energy injection. This scenario was also found to be the case for the short-hard GRB 060313 (Roming et al. 2006).

(iii) Six GRBs sit within $-9 < \alpha_X < -2$, with five sat between $-4.50 < \alpha_X < -2$. The sixth GRB, GRB 050319, has large errors on both the X-ray and optical/UV temporal indices as only two data points fall in the <500 s epoch. Steep decays, such as observed for the five other GRBs ($-4.50 < \alpha_X < -2$), are expected from the tail of the prompt emission (Zhang et al. 2006), suggesting that the X-ray emission of these five GRBs is dominated by prompt emission. These GRBs also have rms deviations that are inconsistent with being zero and hardness ratios that vary rapidly during this epoch, which suggests another jet component or another emission component and so lends support to prompt emission contaminating the X-ray emission. These GRBs are the only GRBs in the sample with X-ray light curves that appear to decay with three of the four segments of the canonical X-ray light curves: an initial steep decay followed by the shallow decay and followed finally by a normal decay. For these GRBs, it appears that as the X-ray temporal index tends to more negative values, the optical/UV temporal index tends to more positive values. However, with only five GRBs, we cannot determine if the X-ray and optical/UV temporal indices of these GRBs are statistically correlated. A larger sample will be required to investigate if a correlation exists.

(iv) Five GRBs lie between $-2 < \alpha_{X,<500\,s} < 0$, but have $\alpha_{O,<500\,s} > 0$. These GRBs are rising in the optical/UV during this early epoch. This behaviour can also be observed by the varying hardness ratios and the inconsistency of the rms deviations with zero for three of these GRBs. For the other two GRBs, the rising behaviour is not observed as clearly as the other GRBs and this is reflected in their hardness ratios and rms deviations. In Oates et al. (2009), the rising behaviour was best explained as to be due to the start of the forward shock. This should be an achromatic effect and therefore should also be observed in the X-ray light curves. Instead what we see is $-2 < \alpha_{X,<500\,s} < 0$, which is usually expected for a light curve after the start of the forward shock. However, from this analysis it is not possible to determine if the rise is masked due to a contribution from the tail of the prompt emission (Zhang et al. 2006) or whether more complex jet geometry is required for these GRBs.

The epoch 500–2000 s is shown in panel (b) of Fig. 3. During this epoch, the GRBs show a slightly higher degree of clustering compared with the previous epoch. The hardness ratios of most GRBs transition from highly variable to relatively constant during this epoch, with the constant phase indicating that the X-ray and optical/UV light curves are produced by a similar mechanism. In panel (b) of Fig. 3, five GRBs are inconsistent with all five lines. The rest of the GRBs are consistent with at least one of the five lines, implying that some GRBs require energy injection. The GRBs are spread evenly above and below the line of equal temporal index, indicating that there is no preference for the type of external medium during this epoch, but a single component outflow can explain most of the GRBs during this time period. For this epoch, the hardness ratios for most GRBs vary more slowly than for the previous epoch and the ratio behaviour in this epoch often continues in to the 2000–20 000 s epoch. This implies that the period between 500 and 2000 s is a transition period where the GRB ceases to have multiple emission mechanisms and emission regions and stabilizes to the late time behaviour.

For the epoch 2000–20 000 s shown in panel (c), we find that all but three GRBs are consistent with $0 < \Delta\alpha \leq 0.50$, with the majority consistent with $\alpha_X + 0.25 \leq \alpha_O \leq \alpha_X + 0.50$. The consistency of most of the GRBs with $\alpha_X + 0.25 \leq \alpha_O \leq \alpha_X + 0.50$ implies that they are satisfied by a constant density medium with a cooling break between the X-ray and optical/UV bands. This is also consistent with what was determined using the mean values, but the consistency with $0.25 < \Delta\alpha \leq 0.50$ implies that energy injection is required for these afterglows, although q does not appear to have one specific value. The rms deviations and the hardness ratios indicate that a single synchrotron spectrum could produce the optical/UV and X-ray light curves because the X-ray and optical/UV light curves behave in a similar way. Four GRBs are inconsistent with lying below the line of equal temporal index, suggesting that these GRBs lie in a wind medium.

For the final epoch, >20 000 s, shown in panel (d), the X-ray temporal indices are typically steeper than observed for the 2000–20 000 s epoch, whereas the range of the optical/UV temporal index has remained the same, implying that for at least some GRBs there is a break in the X-ray light curve. Breaks in the X-ray light curves are also seen through the tendency of the hardness ratio to slowly decrease. The GRBs in the >20 000 s epoch are mostly consistent with $\alpha_X + 0.25 \leq \alpha_O \leq \alpha_X + 0.50$, implying ν_c is between the optical/UV and X-ray bands, the density is constant and that energy injection is still required for some GRBs, although possibly fewer than the previous epoch. The decreasing hardness ratios indicate a significant difference in the behaviour of the X-ray and optical/UV light curves between the 2000–20 000 s epoch and the >20 000 s

epoch, which could be due to the optical/UV and X-ray lying on separate spectral segments. Since in the 2000–20 000 s epoch, the GRBs appear to have an arrangement such that $\nu_m < \nu_O < \nu_c < \nu_X$, it is difficult to produce a decreasing hardness ratio by movement of ν_c, which would move towards either ν_x or ν_o. This would lead to the X-ray and optical/UV light curves lying on the same spectral segment, which would mean they would have the same temporal index and which would lead to a constant hardness ratio rather than a softening one. Some GRBs in the 2000–20 000 s epoch are consistent with the line of equal temporal index, suggesting that either $\nu_m < \nu_O < \nu_X < \nu_c$ or $\nu_m < \nu_c < \nu_O < \nu_X$, the movement of ν_c between the optical/UV and X-ray would therefore cause a softening or a hardening of the hardness ratio, respectively. For those cases where $\nu_m < \nu_O < \nu_c < \nu_X$ the decrease in the hardness ratio may be due to differences in the jet geometry producing the X-ray and optical/UV components or some form of energy injection may be affecting the relative spectrum. Certainly the movement of ν_c can be excluded since the hardness ratio does not converge to become a constant. Finally, in the >20 000 s epoch one GRB, GRB 050730, shows evidence of a jet break, with both the X-ray and optical/UV temporal indices consistent with the post-jet-break temporal relation in Table 4. For GRB 050730, the uncertainties on the optical/UV emission are very large, but the hardness ratio decreases slowly, implying that the break may be chromatic, i.e. occurring only in the X-ray light curve and not the optical/UV light curve.

After 500 s, there appears to be a cooling break between the optical/UV and X-ray bands for most GRBs and a constant density medium is favoured, up to 80–90 per cent of the GRBs in panels (c) and (d) of Fig. 3 are consistent with a constant density medium. The favouritism of the X-ray and optical/UV light curves towards a constant density medium is also shown by Rykoff et al. (2009), who compare average decay rates of the X-ray and optical/UV light curves. Curran et al. (2009) and Panaitescu & Kumar (2002), from samples of six (of a total of 10, see Curran et al. 2009, for further details) and 10 well-studied GRBs, respectively, show that approximately half the GRBs are consistent with constant density medium, which is slightly lower fraction of GRBs than suggested by this work, at least after 2000 s. The higher fraction found in this work and Rykoff et al. (2009) may be due to the systematic fitting approach that both works have taken. As for the relative location of the synchrotron cooling frequency with respect to the optical/UV and X-ray bands, both Curran et al. (2009) and Melandri et al. (2008) independently show that a large fraction of GRBs require a spectral break between the optical/UV and X-ray bands, which is typically expected to be $\nu_O < \nu_c < \nu_X$. Curran et al. (2009) show that out of 10 GRBs, spectral energy distributions (SEDs) of eight could be well constrained and six of these required a spectral break between the X-ray and optical/UV bands, which could be considered to be a cooling break. As for Melandri et al. (2008), they find that 10 GRBs, from their sample of 24, cannot easily be explained by the standard forward shock model. Of the remaining 14 GRBs, seven appear to have $\nu_O < \nu_c < \nu_X$. The fraction of GRBs with $\nu_O < \nu_c < \nu_X$, particularly from Melandri et al. (2008), is lower than that found in this paper, but this paper only considers a difference of $0.25 \leq \Delta\alpha \leq 0.50$ to be due to a cooling frequency and other factors such as multicomponent jets may contaminate our results. Detailed analysis on a GRB by GRB basis must be used to confirm this result.

While the mean temporal indices form a convincing picture from 500 s, an investigation of the individual temporal indices in each epoch introduces new aspects to this picture, for instance additional energy injection. The requirement of energy injection for some GRBs is also observed through comparison of the spectral and temporal indices of the X-ray light curves (Evans et al. 2009). To complete this picture, we must also look at how the individual GRB light curves change in behaviour between the epochs. As observations later than 2000 s are expected to probe the emission produced by the jet after it has begun to plough into the external medium, which surrounds the progenitor, this emission is less likely to be contaminated by emission from the internal shocks. Therefore, we shall examine the change in behaviour between the 2000–20 000 s and >20 000 s epochs.

4.1.3 *Implications of the change in the temporal indices between the 2000–20 000 s and >20 000 s epochs*

In Section 3.3, we found evidence for chromatic breaks in the afterglows of seven GRBs. For all these GRBs, the breaks occur in the X-ray light curves. Support for this chromatic behaviour can be observed in the hardness ratios as a softening, which occurs when the X-ray breaks to a steeper decay, while the optical/UV light curve continues to decay at the same rate. The change in the X-ray temporal index and the evolution of the hardness ratios provides strong support for chromatic breaks. However, we do caution that a break in the optical/UV light curve at late times cannot be excluded without detailed investigation of the afterglows. For each of the seven GRBs, we fit a power law and a broken power law to the X-ray light curve from 1000 s and onwards. If the broken power law was the best fit we continued to test if a break in the optical/UV light curve could be consistent with the X-ray break. To do this we fit a broken power law to the optical/UV light curve from 1000 s onwards, fixing the difference in the temporal index of the two decay segments to be the same as found for the X-ray broken power-law fit. We then determined the earliest time at which the optical/UV light curve could break and whether this time is consistent with the break in the X-ray light curve. We shifted the break time of the fit to the optical light curve so that the χ^2 changed by $\Delta\chi^2 = 9$ (i.e. 3σ). If the resulting break time is consistent with the X-ray break time, then the we cannot be certain that the X-ray break is chromatic. Out of the seven GRBs, five are best fit by a broken power law in the X-ray. The two other GRBs, GRB 060804 and GRB 060908, could not be fit by a broken power law due to the break occurring before or to close to 1000 s. Of the five GRBs with X-ray light curves best fit by a broken power law, we are able to convincingly demonstrate that three GRBs (GRB 050319, GRB 051109a and GRB 060206) have a chromatic break, with the 3σ upper limit to an optical break time much later than the X-ray break time.

Achromatic breaks may not truly be achromatic and hence may appear as chromatic breaks. van Eerten et al. (2010) have shown through simulations that jet breaks, or any variability due to changes in the fluid conditions, may be chromatic, typically occurring later in radio bands than in the X-ray or optical. They claim that for certain physical parameters X-ray and optical jet breaks (or variability) may occur at different times, although the difference is not well pronounced between these two bands. Simulations have also shown that jet breaks may also not be so sharp for lower frequencies compared to higher frequencies due to limb brightening effects (Granot, Piran & Sari 1999; van Eerten et al. 2010). This is expected to be most pronounced for X-ray/optical versus radio, with the radio emission having the smoothest break. However, the difference in smoothness between the X-ray and optical/UV is expected to be less pronounced especially if they lie on the same spectral segments,

but there may be some difference if ν_c lies between the two bands. Some achromatic breaks may be confused with chromatic breaks due to these effects, however, these effects are likely to cause only minor differences in the break times of the optical/UV and X-ray light curves.

Racusin et al. (2009) have shown that there is no X-ray spectral evolution after 2000 s, therefore breaks which are only observed in the X-ray light curve must be due to one of four possibilities: variations in the micro-physical parameters (Panaitescu et al. 2006) – which is rather contrived; changes in the external medium – such as was suggested as an alternative explanation for GRB 080319B (Racusin et al. 2008); cessation of energy injection; a jet break. The change in the external medium specifically from a constant density to a wind-like medium or vice versa would be shown in Fig. 5 by the GRBs crossing the line of equal temporal index. A position above the line implies an ISM-like medium and a position below the line implies a wind-like medium. None of the GRBs with chromatic breaks has temporal indices that cross the line of equal temporal index, implying that at least at a simplistic level, the change in density of the external medium, from wind-like to constant density or vice versa, cannot explain the chromatic break. However, this paper has not investigated the relations where $1 < p < 2$ nor has it investigated complex variations in the external density. If we simply apply the closure relations for a constant density medium with $\nu_m < \nu_O < \nu_c < \nu_X$ to the X-ray and optical/UV temporal indices from the 2000–20 000 s and >20 000 s epochs for these seven GRBs, then we find for the X-rays p is consistent within 1σ errors with ≥ 2 for five GRBs in the 2000–20 000 s epoch and ≥ 2 for all seven GRBs in the >20 000 s epoch. For the optical only three GRBs are consistent within 1σ errors with $p \geq 2$ in the 2000–20 000 s epoch and three are consistent in the >20 000 s epoch. While this may indicate the $1 < p < 2$ closure relations should be examined, the values of p will increase to $p > 2$ if values of q, the energy injection parameter, are reduced from 1. Since the $1 < p < 2$ closure relations and changing external media are more complex options they cannot be ruled out by this work, but shall not be investigated further here. The last two possibilities, cessation of energy injection and a jet break, would produce achromatic breaks in a single component outflow. In these cases, changes in temporal index of the optical/UV light curves are expected, but these changes are not seen. Therefore, the chromatic breaks observed in the X-ray light curves are difficult to explain in terms of a single component outflow. Chromatic breaks in several GRBs, which were observed in the X-ray and not the optical/UV (including GRB 050319 and GRB 050802) have been investigated by Oates et al. (2007) and De Pasquale et al. (2009), who also found that a single component outflow could not explain the observations.

For two GRBs, the temporal indices determined from the epochs 2000–20 000 s and >20 000 s lie on different sides of the line of equal temporal index, suggesting a change in external density. GRB 061021 crosses from above to below the line of equal temporal index, which implies a transition between constant density medium to wind-like medium. Conversely, GRB 070318 crosses from below to above the line of equal temporal index, which implies a transition between a wind-like medium to a constant density medium. The change in external density essentially changes the frequency of ν_c (see Zhang & Mészáros 2004, for equations describing ν_c in wind-like and constant density media). For GRB 061021, the X-ray and optical/UV temporal indices, determined from the epochs 2000–20 000 s and >20 000 s, both change by $\geq 3\sigma$ and are not consistent with each other. These temporal indices cannot be explained by the non-energy injected temporal relations in Table 4 with a change in density from constant to wind-like. GRB 070318 is also inconsistent with a change in external medium this time from wind-like to constant density because the change from wind-like non-energy-injected temporal relations to constant density non-energy-injected temporal relations does not allow the X-ray light curves to become steeper while the optical/UV light curves become shallower. Therefore, it is difficult to explain why for two GRBs the temporal indices, determined from the epochs 2000–20 000 s and >20 000 s, lie on different sides of the line of equal temporal index. However, the investigation of external density variations may be too simplistic because the external density may have a different density profile and may be highly variable. Temporal relations for $1 < p < 2$ have also not been examined. For $1 < p < 2$, the temporal indices describing the frequency $\nu_c < \nu$ are different for the constant density and wind-like media. This implies that the X-ray and optical/UV temporal indices would always be expected to change, unlike for the $p > 2$ case. The $1 < p < 2$ case may be able to explain the behaviour of some of the other GRBs in the sample, especially those that appear to have density changes.

Ultimately, it is difficult to reconcile the optical/UV and X-ray observations of some GRBs in terms of a single component jet. We shall now look at more complex geometric models to determine if these can explain the observations.

4.2 Additional emission components

Additional emission components come in two main flavours, either the jet consists of two (or more) components or there is some form of additional energy injection, such as up-scattered forward shock emission (Panaitescu 2008) or late 'prompt' emission (Ghisellini et al. 2007, 2009).

In a two component jet, there are two theoretical ways in which the optical/UV and X-ray emission can be produced. Either the narrow component, with the higher Lorentz factor, produces the X-ray emission and the slower, wider component produces the optical/UV emission (Oates et al. 2007; De Pasquale et al. 2009) or the narrow and wide components produce both X-ray and optical/UV emission (Huang et al. 2004; Peng, Königl & Granot 2005; Granot, Ramirez-Ruiz & Perna 2005). The simplest scenario is that both components produce X-ray and optical/UV emission. However, Oates et al. (2009) ruled out the possibility because the viewer would observe two peaks from the two different emission components. This effect is not seen in the UVOT light curves, and therefore the jet is unlikely to have two components where both produce optical/UV emission.

The second two component jet scenario is that the optical/UV emission is produced by the wide component and the X-ray emission is produced by the narrow component. A discussion of how the wide component can produce emission predominantly in the optical/UV without contaminating the X-ray and how the narrow component can produce emission predominantly in the X-ray without contaminating the optical/UV is provided in De Pasquale et al. (2009). In this scenario, the X-ray and optical/UV light curves are not required to be produced by the same synchrotron spectrum. However, the X-ray and optical/UV afterglows should be satisfied by the temporal relations for the same external medium, either wind-like or ISM-like.

In the up-scattered emission model, the up-scattered emission is thought to be due to photons in the forward shock, which travel away from the forward shock towards the outflow. These photons are scattered by interactions with either hot or cold electrons in the outflow (Panaitescu 2008). If the interactions are with hot electrons,

then the scattering will be Inverse Compton and seed photons of low energy, and will be boosted in to the X-rays. If the interactions are with cold electrons, then the photons will not gain energy, so a large number of seed photons will be required to be scattered to produce sufficient flux to be brighter than the flux of the forward shock. A second effect may cause the up-scattered emission to be brighter than the forward shock. If the photons produced at the same time as those in the forward shock are up-scattered and received by the observer at a later time after the afterglow has begun to decay, then the scattered flux arriving later may be brighter than the forward shock-flux at that time; see Panaitescu (2008) for further details. Overall the X-ray and optical light curves may be a combination of various degrees of flux contributed from both the forward shock and scattering, which enables this model to reproduce flares, plateaus and chromatic breaks. In the case of chromatic breaks, it would require the scattered emission to cease contributing to the X-ray light curve at the break time, which may be difficult to explain. This model has many possibilities for the effect of scattered emission. The scattered emission may either not contribute strongly to both the X-ray or optical afterglow, it may contribute strongly to just the X-ray emission, or it may contribute strongly to both the X-ray and optical emission. An indication that the scattered emission is dominant over the forward shock emission will be a plateau in the observed light curves.

In the late 'prompt' emission scenario, the central engine is assumed to be active for a period longer than the duration of the prompt emission. The central engine steadily produces shells of material at lower and lower Lorentz factors, which by internal dissipation produce continuous and smooth emission predominantly in the X-rays, but possibly also in the optical/UV (Ghisellini et al. 2007, 2009). The addition of the late 'prompt' emission to the afterglow emission allows a wide range of temporal indices and also allows the model to reproduce a wide range of X-ray and optical/UV temporal behaviour including chromatic breaks.

As the late 'prompt' emission and the up-scattered emission models predict light curves that are a combination of two different emission components, with varying degrees of contribution from the two components, it is not possible analytically to determine if these model are acceptable. However, this wide range in behaviour implies that these scenarios are temporally indistinguishable from the two component outflow model. Therefore, in the following we shall talk primarily of whether the two component model can explain our observations.

When investigating the single component outflow, we found that the synchrotron cooling frequency typically lies in between the X-ray and optical/UV bands, that energy injection may be required for some GRBs, and that there is conclusive evidence for a chromatic break in three GRBs and evidence for chromatic breaks occurring in four further GRBs. These breaks occur in the X-ray and cannot easily be explained by a single component outflow. They cannot be explained by a direct change in the external density (although complex variation cannot be ruled out), nor by the passage of ν_c through the X-ray band because X-ray spectral evolution is not observed during the late afterglow (Racusin et al. 2009). Therefore, as discussed in Section 4.1.3, we consider this break to be due to either the cessation of energy injection or a jet break. In a two component outflow, we would expect energy to be injected into both components. However, it is difficult to picture the break in the X-rays being caused by the cessation of energy injection in the narrow component only, although from this analysis it cannot be ruled out completely. Therefore, we take the jet break in the narrow component to be the cause of the change in X-ray temporal index (De Pasquale et al. 2009). However, if this is the case then the X-ray temporal indices after >20 000 s are shallower than expected for the uninjected decay post-jet-break temporal relations (Table 4). The fourth segment of the X-ray light curve which is considered to be the true post-jet-break phase is also shallower than expected (Evans et al. 2009). The inclusion of energy injection will cause the temporal decay index before and after the jet break to be less steep. This would be a natural conclusion because energy injection has already been shown to be needed to explain the afterglow behaviour of some GRBs. The post-jet-break temporal indices from the values predicted in Table 4 will be reduced by the quantities determined from equations (33), (34) and (35) of Panaitescu et al. (2006). For the simplest jet, a jet with sharp edges which spreads laterally, the temporal index of the post-jet-break decay is reduced from $\alpha \sim -p$ by $\Delta\alpha = (2/3)\ (1 - q)(1 - \beta)$ for $\nu_c < \nu_X$. Taking $\beta = -p/2$, the range in $\Delta\alpha$ is 1.33, 1.66 for $q = 0$ and $p = 2$, 3 to $\Delta\alpha = 0.0$, 1.0 for $q = 1$ and $p = 2$, 3. For $p = 2$–3, this produces a range $-0.66 < \alpha < -3$ for the post-jet-break decay. This relation alone can explain the X-ray temporal indices of all GRBs for the >20 000 s epoch in Table 1. The jet may also not show any sideways expansion; in this case the jet is reduced from $\alpha = 3/2\beta - [(2 - s)/(8 - 2s)]$ by $\Delta\alpha = 1/2(1 - q)(1 - \beta) + [1/(4 - s)]$ for $\nu_c < \nu_X$ (Panaitescu et al. 2006). Again taking $\beta = -p/2$ and $s = 0$, indicating a constant density medium, the range in $\Delta\alpha$ is 1.25, 1.50 for $q = 0$ and $p = 2$, 3 to $\Delta\alpha = 0.25$ for $q = 1$ and $p = 2$, 3. For $p = 2$–3, this produces a range $0 < \alpha < -1.75$ for the post-jet-break decay. This is acceptable for the optical/UV and X-ray temporal indices for the GRBs in the >20 000 s epoch. If the post-jet-break decay is energy injected, then we would expect the 2000–20 000 s decay to be also energy injected. In this case, the range of temporal indices expected for the 2000–20 000 s epoch is given by the energy injected temporal relations in Table 4 to be $-1.90 < \alpha < 0.5$, which is consistent with the temporal indices determined in this period given in Table 1.

This appears to be a plausible explanation for the optical/UV and X-ray temporal behaviour of the GRBs with chromatic breaks. The wide range of possible temporal indices allowed by the fact the X-ray and optical/UV emission are decoupled implies that the two component model could be used to explain a larger number of GRBs, if not all GRBs. However, a comprehensive investigation of the spectral and temporal properties of GRBs is required to determine if one of the additional emission mechanisms is able to reproduce all GRB observations.

5 CONCLUSIONS

In this paper we systematically analysed a sample of 26 UVOT and XRT observed GRB light curves. We found that the behaviour of the optical/UV and X-ray light curves is most different during the early afterglow before 500 s, and that the light curves behave most similarly during the middle phase of the afterglow between 2000 and 20 000 s.

The mean temporal indices of the optical/UV and X-ray light curves determined from three epochs after 500 s, imply that the average X-ray and optical/UV afterglow is produced by slow cooling electrons, in a constant density medium with the synchrotron cooling frequency set between the optical/UV and X-ray bands. However, when we look at the individual GRBs, the picture is not so simple. While these properties generally well describe the outflow of the individual GRBs from 500 s and onwards, this picture requires energy injection to explain the temporal indices of some of the GRB outflows. The need for energy injection is shown by

the difference in the optical/UV and X-ray temporal indices, which require a difference of $0.25 \leq \Delta\alpha \leq 0.50$, where a difference of 0.25 would be expected for non-injected afterglows and 0.50 is the maximum difference expected when energy injection is included.

We demonstrated that a chromatic break occurs in the afterglows of three GRBs (GRB 050319, GRB 051109a and GRB 060206), while for a further four GRB afterglows we have strong indications of chromatic breaks. These breaks are observed in the X-ray light curves as a steepening of the X-ray temporal index between 2000 and 10^5 s and a softening of their hardness ratios. The lack of X-ray spectral evolution (Racusin et al. 2009) implies these breaks are likely to be caused either by changes in the external density, a jet break or is due to the cessation of energy injection. We determined that the density evolution on a simplistic scale is not the cause of chromatic breaks, but at this stage we cannot rule out complex density evolution. Both the jet break and cessation of energy injection would produce an achromatic break if the jet is a single component uniform jet. We have shown that chromatic breaks can either be produced if the X-ray and optical/UV emission are decoupled and produced in a jet with structure, for instance in a two component jet where the narrow component produces the X-ray emission and the wide component produces the optical/UV emission, or it may be produced in the late 'prompt' emission model or the up-scattered emission model.

ACKNOWLEDGMENTS

This research has made use of data obtained from the High Energy Astrophysics Science Archive Research Center (HEASARC) and the Leicester Data base and Archive Service (LEDAS), provided by NASA's Goddard Space Flight Center and the Department of Physics and Astronomy, Leicester University, UK, respectively. This work made use of data supplied by the UK Swift Science Data Centre at the University of Leicester. SRO acknowledges the support of an STFC Studentship. MJP, MDP, PAC, NPMK, PAE and KLP acknowledge the support of STFC, and SZ thanks STFC for its support through an STFC Advanced Fellowship. MMC, TSK, JAN, PWAR and MHS acknowledge support through NASA contract NAS5-00136. We also thank the referee for useful comments and suggestions.

REFERENCES

Barthelmy S. D. et al., 2005, Space Sci. Rev., 120, 143
Berger E., Kulkarni S. R., Rau A., Fox D. B., 2006, GRB Coordinates Network, 4815, 1
Berger E., Fox D. B., Cucchiara A., 2007, GRB Coordinates Network, 6470, 1
Bloom J. S., Foley R. J., Koceveki D., Perley D., 2006, GRB Coordinates Network, 5217, 1
Bloom J. S., Perley D. A., Chen H. W., 2006, GRB Coordinates Network, 5826, 1
Burrows D. N. et al., 2005, Space Sci. Rev., 120, 165
Chen H.-W., Thompson I., Prochaska J. X., Bloom J., 2005, GRB Coordinates Network, 3709, 1
Chevalier R. A., Li Z., 2000, ApJ, 536, 195
Curran P. A., Starling R. L. C., van der Horst A. J., Wijers R. A. M. J., 2009, MNRAS, 395, 580
Curran P. A., Evans P. A., de Pasquale M., Page M. J., van der Horst A. J., 2010, ApJ, 716, L135
Dai Z. G., Cheng K. S., 2001, ApJ, 558, L109
De Pasquale M. et al., 2009, MNRAS, 392, 153
Evans P. A. et al., 2007, A&A, 469, 379
Evans P. A. et al., 2009, MNRAS, 397, 1177
Falcone A. D. et al., 2007, ApJ, 671, 1921
Foley R. J., Chen H.-W., Bloom J., Prochaska J. X., 2005, GRB Coordinates Network, 3483, 1
Fynbo J. P. U. et al., 2005, GRB Coordinates Network, 3749, 1
Fynbo J. P. U., Limousin M., Castro Cerón J. M., Jensen B. L., Naranen J., 2006, GRB Coordinates Network, 4692, 1
Ghisellini G., Ghirlanda G., Nava L., Firmani C., 2007, ApJ, 658, L75
Ghisellini G., Nardini M., Ghirlanda G., Celotti A., 2009, MNRAS, 393, 253
Granot J., Piran T., Sari R., 1999, A&AS, 138, 541
Granot J., Ramirez-Ruiz E., Perna R., 2005, ApJ, 630, 1003
Huang Y. F., Wu X. F., Dai Z. G., Ma H. T., Lu T., 2004, ApJ, 605, 300
Jakobsson P., Levan A., Chapman R., Rol E., Tanvir N., Vreeswijk P., Watson D., 2006a, GRB Coordinates Network, 5617, 1
Jakobsson P., Fynbo J. P. U., Tanvir N., Rol E., 2006b, GRB Coordinates Network, 5716, 1
Jakobsson P. et al., 2006c, A&A, 460, L13
Jaunsen A. O., Fynbo J. P. U., Andersen M. I., Vreeswijk P., 2007, GRB Coordinates Network, 6216, 1
Kouveliotou C., Meegan C. A., Fishman G. J., Bhat N. P., Briggs M. S., Koshut T. M., Paciesas W. S., Pendleton G. N., 1993, ApJ, 413, L101
Ledoux C., Vreeswijk P., Smette A., Jaunsen A., Kaufer A., 2006, GRB Coordinates Network, 5237, 1
Liang E.-W., Zhang B.-B., Zhang B., 2007, ApJ, 670, 565
Maccacaro T., Gioia I. M., Wolter A., Zamorani G., Stocke J. T., 1988, ApJ, 326, 680
Markwardt C. B., 2009, in Boehlender D., Durand D., Dowler P., eds, ASP Conf. Ser. Vol. 411, Non-linear Least-squares Fitting in IDL with MPFIT. p. 251
Melandri A. et al., 2008, ApJ, 686, 1209
Meszaros P., Rees M. J., Wijers R. A. M. J., 1998, ApJ, 499, 301
Nousek J. A. et al., 2006, ApJ, 642, 389
Oates S. R. et al., 2007, MNRAS, 380, 270
Oates S. R. et al., 2009, MNRAS, 395, 490
Panaitescu A., 2008, MNRAS, 383, 1143
Panaitescu A., Kumar P., 2002, ApJ, 571, 779
Panaitescu A., Mészáros P., Gehrels N., Burrows D., Nousek J., 2006, MNRAS, 366, 1357
Panaitescu A., Mészáros P., Burrows D., Nousek J., Gehrels N., O'Brien P., Willingale R., 2006, MNRAS, 369, 2059
Peng F., Königl A., Granot J., 2005, ApJ, 626, 966
Peterson B., Schmidt B., 2006, GRB Coordinates Network, 5223, 1
Prochaska J. X., Chen H.-W., Bloom J. S., Falco E., Dupree A. K., 2006, GRB Coordinates Network, 5002, 1
Quimby R., Fox D., Hoeflich P., Roman B., Wheeler J. C., 2005, GRB Coordinates Network, 4221, 1
Racusin J. L. et al., 2008, Nat, 455, 183
Racusin J. L. et al., 2009, ApJ, 698, 43
Rol E., Jakobsson P., Tanvir N., Levan A., 2006, GRB Coordinates Network, 5555, 1
Roming P. W. A. et al., 2005, Space Sci. Rev., 120, 95
Roming P. W. A. et al., 2006, ApJ, 651, 985
Rykoff E. S. et al., 2009, ApJ, 702, 489
Sakamoto T. et al., 2008, ApJS, 175, 179
Sari R., Piran T., Narayan R., 1998, ApJ, 497, L17
Sari R., Piran T., Halpern J. P., 1999, ApJ, 519, L17
Starling R. L. C., van der Horst A. J., Rol E., Wijers R. A. M. J., Kouveliotou C., Wiersema K., Curran P. A., Weltevrede P., 2008, ApJ, 672, 433
van Eerten H. J., Meliani Z., Wijers R. A. M. J., Keppens R., 2010, MNRAS, doi:10.1111/j.1365-2966.2010.17582.x
Zhang B., Mészáros P., 2001, ApJ, 552, L35
Zhang B., Mészáros P., 2004, Int. J. Modern Phys. A, 19, 2385
Zhang B., Fan Y. Z., Dyks J., Kobayashi S., Mészáros P., Burrows D. N., Nousek J. A., Gehrels N., 2006, ApJ, 642, 354

This paper has been typeset from a TEX/LATEX file prepared by the author.